Basal forebrain volume selectively and reliably predicts the cortical spread of Alzheimer's degeneration

Sara Fernández-Cabello[1,2], Martin Kronbichler[1,2,3], Koene R. A. Van Dijk[4], James A. Goodman[4], R. Nathan Spreng[5,6,7], Taylor W. Schmitz[8,9] for the Alzheimer's Disease Neuroimaging Initiative*

[1] Department of Psychology, University of Salzburg, Salzburg, Austria
[2] Centre for Cognitive Neuroscience, University of Salzburg, Salzburg, Austria
[3] Neuroscience Institute, Christian-Doppler Medical Centre, Paracelsus Medical University, Salzburg, Austria.
[4] Clinical and Translational Imaging, Early Clinical Development, Pfizer Inc, Cambridge, MA, United States
[5] Laboratory of Brain and Cognition, Montreal Neurological Institute, Department of Neurology and Neurosurgery, McGill University, Montreal, QC, Canada
[6] Departments of Psychiatry and Psychology, McGill University, Montreal, QC, Canada
[7] Douglas Mental Health University Institute, Verdun, QC, Canada
[8] Brain and Mind Institute, Western University, London, ON, Canada
[9] Department of Physiology and Pharmacology, Western University, London, ON, Canada

* Data used in preparation of this article were obtained from the Alzheimer's Disease Neuroimaging Initiative (ADNI) database (adni.loni.usc.edu). As such, the investigators within the ADNI contributed to the design and implementation of ADNI and/or provided data but did not participate in analysis or writing of this report. A complete listing of ADNI investigators can be found at: http://adni.loni.usc.edu/wp-content/uploads/how_to_apply/ADNI_Acknowledgement_List.pdf

Abstract

Alzheimer's disease neuropathology is thought to spread across anatomically and functionally connected brain regions. However, the precise sequence of spread remains ambiguous. The prevailing model posits that Alzheimer's neurodegeneration starts in the entorhinal cortices, before spreading to temporoparietal cortex. Challenging this model, we previously provided evidence that degeneration within the nucleus basalis of Meynert (NbM), a subregion of the basal forebrain heavily populated by cortically projecting cholinergic neurons, precedes and predicts entorhinal degeneration (Schmitz and Spreng, 2016). There have been few systematic attempts at directly comparing staging models using in vivo longitudinal biomarker data, and determining if these comparisons generalize across independent samples. Here we addressed the sequence of pathological staging in Alzheimer's disease using two independent samples of the Alzheimer's Disease Neuroimaging Initiative (*N1* = 284; *N2* = 553) with harmonized CSF assays of amyloid (Aβ) and hyperphosphorylated tau (pTau), and longitudinal structural MRI data over two years. We derived measures of gray matter degeneration in a priori NbM and the entorhinal regions of interest. To examine the spreading of degeneration, we used a predictive modelling strategy which tests whether baseline gray matter volume in a seed region accounts for longitudinal change in a target region. We demonstrated that predictive pathological spread favored the NbM→entorhinal over the entorhinal→NbM model. This evidence generalized across the independent samples (*N1*: r=0.20, p=0.03; *N2*: r=0.37, p<0.001). We also showed that CSF concentrations of pTau/Aβ moderated the observed predictive relationship, consistent with evidence in rodent models of an underlying trans-synaptic mechanism of pathophysiological spread (t_{826}=2.55, p=0.01). The moderating effect of CSF was robust to additional factors, including clinical diagnosis (t_{826}=1.65, p=0.49). We then applied our predictive modelling strategy to an exploratory whole-brain voxel-wise analysis to examine the spatial specificity of the NbM→entorhinal model. We found that smaller baseline NbM volumes predicted greater degeneration in localized regions of the entorhinal and perirhinal cortices. By contrast, smaller baseline entorhinal volumes predicted degeneration in the medial temporal cortex, recapitulating the prevailing staging model. Our findings suggest that degeneration of the basal forebrain cholinergic projection system is a robust and reliable upstream event of entorhinal and neocortical degeneration, calling into question the prevailing view of Alzheimer's disease pathogenesis.

Keywords: Alzheimer's disease, basal forebrain, NbM, EC

Abbreviations

aCSF	Abnormal CSF group based on the pTau/A$\beta_{1\text{-}42}$ ratio >= 0.28
ADNI	Alzheimer's Disease Neuroimaging Initiative
APC	Annual Percent Change
Aβ	Amyloid Beta
BF	Basal forebrain
EC	Entorhinal Cortex
GM	Gray Matter
NbM	Nucleus Basalis of Meynert
nCSF	Normal CSF group based on the pTau/A$\beta_{1\text{-}42}$ ratio <0.28
pTau	Hyper phosphorylated tau
sMRI	Structural MRI
ROI	Region of Interest
TGM	Total Gray Matter
TICV	Total Intracranial Volume

Introduction

Alzheimer's disease neuropathology progresses in stages, with certain brain regions affected by neuronal deposition of insoluble amyloid (Aβ) and hyper phosphorylated tau (pTau) before others. The asymmetrical progression of Alzheimer's disease neuropathology in different brain regions may reflect selective neuronal vulnerabilities local to each region (Mattson and Magnus, 2006; Saxena and Caroni, 2011; Wu *et al.*, 2014; Schmitz and Nathan Spreng, 2016). However, evidence in both mouse models of Alzheimer's disease (De Calignon *et al.*, 2012; Liu *et al.*, 2012) and in human Alzheimer's disease patients (Schmitz *et al.*, 2018; Sepulcre *et al.*, 2018) indicates that neuropathology also spreads across anatomically and functionally connected brain regions. It is therefore possible that pathologies arising from selective neuronal vulnerability local to a given brain region might precede and predispose the subsequent spread of pathology across networks (Warren *et al.*, 2013). Despite these observations, the precise sequence of neuropathological spread and its relationship with neurodegeneration during the earliest stages of disease remains ambiguous, and can only be resolved with in vivo longitudinal data integrating measures of proteinopathy and microstructural change. Moreover, there have been few systematic attempts at generalizing staging models across independent samples, which limits their clinical utility. Determining when and why certain brain regions are affected in the course of Alzheimer's disease is essential for understanding the mechanistic basis of disease progression, accurately staging the disease, and identifying individuals for early therapeutic interventions.

The prevailing staging model posits that abnormal Aβ and pTau accumulation starts in the entorhinal cortices (Braak and Braak, 1991; Corder *et al.*, 2000; Braak *et al.*, 2006), before spreading to interconnected areas of medial temporal and posterior parietal cortex. The selective vulnerability of neurons in the entorhinal cortex to these proteinopathies is attributed to their high metabolic activity, the complexity of their axonal projections and the lifelong maintenance of their axonal plasticity (Mattson and Magnus, 2006; Liu *et al.*, 2012; Khan *et al.*, 2014; Wu *et al.*, 2014; Roussarie *et al.*, 2018). One individual spiny stellate neuron in layer II of the entorhinal cortex innervates the entire transverse axis of the dentate gyrus, CA2/CA3 and the subiculum (Tamamaki and Nojyo, 1993). Under a recent framework, amyloid pathology in entorhinal neurons potentiates hyper-phosphorylation of tau proteins ; Khan *et al.*, 2014; Wu *et al.*, 2016), which then spread via

trans-synaptic mechanisms to distal neocortical areas which receive inputs from EC; i.e. the EC→Neocortical model. See Figure 1A.

Challenging the EC→Neocortical model, we have provided initial evidence that degeneration within the nucleus basalis of Meynert (NbM), a subregion of the basal forebrain, precedes and predicts degeneration in the EC (Schmitz and Spreng, 2016). The NbM (also referred to as Ch4 in Mesulam's nomenclature (Mesulam, 1983; Mesulam and Geula, 1988) is heavily populated (90% of cell bodies) by cortically projecting cholinergic neurons (Mesulam *et al.*, 2004) which are also known for their extremely long and complex branching; the full arborization length of a single neuron was estimated in humans at >100 meters (Wu *et al.*, 2014). Like the layer II entorhinal spiny projection neurons, the cortical cholinergic projection neurons of the basal forebrain accumulate Aβ and pTau early in the course of Alzheimer's disease, and as early as the third decade of life (Mesulam *et al.*, 2004; Baker-Nigh *et al.*, 2015). Lending further support to early vulnerability of the basal forebrain to Alzheimer's disease, we previously found that longitudinal NbM degeneration was selectively increased in cognitively normal older adults with abnormal CSF biomarkers of Aβ, over and above age-related degeneration in cortical areas including entorhinal cortex (Schmitz and Spreng, 2016). These initial findings raise the possibility that Alzheimer's disease pathology spreads from the basal forebrain to entorhinal cortex (NbM→EC), possibly via the same trans-synaptic mechanisms of tau spread proposed previously in the rodent research (Liu *et al.*, 2012). If true, the NbM→EC model would add a crucial 'upstream' link to the EC→Neocortical predictive pathological staging of Alzheimer's disease. Under this model, the ascending cholinergic projections from NbM first 'seed' the EC with tau pathology, thereby eventuating the pattern of temporoparietal neurodegeneration typically attributed to the earliest stages of Alzheimer's disease. Support for the NbM→EC model would have major clinical implications, motivating a shift toward preventative treatment strategies aimed at relieving age-related pressures on the cortical cholinergic projection system.

Here we directly compared the NbM→EC and EC→NbM models of predictive pathological staging in a large sample of older adults ranging from cognitively normal to Alzheimer's dementia, and then examined if the results generalized to a second independent sample of adults spanning the same clinical diagnostic continuum. In each sample, we first integrated CSF biomarkers of Aβ and pTau neuropathology into a ratio pTau/AB and delineate two groups of older adults in each of

the two samples using an independently defined ratio cutpoint which was recently cross-validated at ~90% sensitivity and specificity (Hansson 2018, Schindler 2018). Individuals below the cutpoint exhibit a 'neurotypical' biomarker-based phenotype of brain aging; individuals above the cutpoint exhibit an 'Alzheimer's pathological' phenotype. Because CSF pTau/AB is sensitive to the earliest abnormalities of AD (Jack et al 2013), we identified many cognitively normal adults falling above the cutpoint in both samples. We then tracked these groups with structural MRI (sMRI) indices of baseline gray matter volume and longitudinal neurodegeneration over a two-year period. Both the CSF and sMRI data were acquired from multiple phases of the Alzheimer 's disease Neuroimaging Initiative (ADNI).

To examine the 'spread' of degeneration between NbM and EC, we used a predictive modelling strategy which tests whether baseline gray matter volume in a seed region accounts for variation in subsequent longitudinal degeneration (change over future timepoints) in a target region. We determined whether evidence of predictive pathological spread favored either the NbM→EC or EC→NbM model, and whether this evidence generalized across the independent samples. We then determined whether CSF concentrations of pTau/Aβ moderated the observed predictive relationship, consistent with an underlying trans-synaptic mechanism of pathophysiological spread. Additional moderating factors, including clinical diagnosis, were evaluated in this framework. We then examined the selectivity of predictive pathological spread between NbM and EC using a whole-brain voxel-wise predictive modelling strategy. Finally, we used the same whole-brain strategy to test whether the EC→Neocortical model recapitulates the spread of neuropathology from EC to temporoparietal cortices observed in prior work (Liu *et al.*, 2012; Khan *et al.*, 2014). If degeneration in the basal forebrain cholinergic projection system is a robust and reliable upstream event of entorhinal degeneration, then it should predict localized entorhinal degeneration, whereas entorhinal cortex should predict downstream events in temporal and parietal cortices.

Methods

ADNI Data

Data used in the preparation of this article were obtained from the Alzheimer's Disease Neuroimaging Initiative (ADNI) database (adni.loni.usc.edu). The ADNI was launched in 2003 as a public-private partnership, led by Principal Investigator Michael W. Weiner, MD. The primary goal of ADNI has been to test whether serial magnetic resonance imaging (MRI), positron emission tomography (PET), other biological markers, and clinical and neuropsychological assessment can be combined to measure the progression of mild cognitive impairment (MCI) and early Alzheimer's disease (AD).

We used data from the ADNI-1 as first cohort and ADNI-GO and ADNI-2 combined (ADNI-GO/2) as second cohort. ADNI-1 was carried out in 1.5T MR scanners and ADNI-GO/2 in 3T MR scanners. All high-resolution T1 sMRI scans were downloaded from ADNI LONI (http://adni.loni.usc.edu/). A total of 502 ADNI-1 sMRI scans were downloaded from a standardized 2-years interval image collection. This data collection was created to minimize variability between studies and ensure a minimum quality control of the images (Wyman *et al.*, 2014). To obtain the ADNI-GO/2 sMRI scans, we first selected those subjects that had CSF biomarker data (see below) and searched by their research IDs (RIDs). We downloaded longitudinal sMRI images from 714 ADNI-GO/2 participants. To select the two longitudinal time points for each individual, we applied a bounded interval of a mean=1.5 years +/- 12 months to maximize the inclusion of participants. 104 participants didn't have longitudinal sMRI data within the bounded interval. For ADNI sites with GE and Siemens scanners, we used images corrected for distortions (GradWarp) and B1 non-uniformity. For ADNI sites with Philips scanners, these corrections are applied at acquisition (see http://adni.loni.usc.edu/methods/mri-tool/mri-pre-processing/). Finally, to be able to compare ADNI-1 and ADNI-GO/2 data as two independent samples, we discarded participants from ADNI-GO/2 that also took part in the ADNI-1 studies (n=49), due to the smaller sample size of the ADNI1 cohort.

CSF biomarkers

Accumulation of brain Aβ in plaques and pTau in neurofibrillary tangles are the main neuropathological signs of AD. These biomarkers can be measured in the CSF and are able to differentiate Alzheimer's disease patients in good concordance with positron emission tomography classifications (Shaw *et al.*, 2009; Hansson *et al.*, 2018; Schindler *et al.*, 2018). CSF samples of Aβ and pTau from the baseline visit were produced with a fully-automated Elecsys protocol (see Supplementary section *CSF procedures*). We calculated a ratio of pTau/Aβ and used a standardized cut-off of 0.028, which was recently cross-validated between the ADNI and Swedish BioFinder studies (Hansson *et al.*, 2018) to classify participants into abnormal (aCSF; pTau/Aβ >= 0.028) and a normal CSF groups (nCSF < 0.028). Using ratios of pTau over Aβ supersedes using single analytes to distinguish amyloid status using positron emission tomography (Schindler *et al.*, 2018). 216 participants from ADNI-1 didn't have CSF measures and were therefore not included. It is important to note that our grouping strategy is purely based on CSF biomarkers, independent of any cognitive or clinical diagnosis, though we follow-up with analyses of clinical diagnosis (see Results).

APOE genotyping

The ε4 allele of the APOE gene is the strongest genetic risk factor for non-familial Alzheimer's disease (Corder *et al.*, 1993; Liu and Bu, 2013) and is thought to interact with the selective vulnerability of cholinergic BF neurons by disrupting the capacity of these cells to support and maintain their enormous axonal membranes (Poirier *et al.*, 1993, 1995; Poirier, 1994). In order to study the effect of the CSF Alzheimer's disease biomarkers independently of other factors, we included the APOE genotype as a covariate of no interest in our analyses. The APOE information for all individuals with both sMRI and CSF data was obtained from the APOERES.csv spreadsheet and the ε4+ status was defined as having at least one ε4 allele. A blood sample at the screening or baseline visit was collected for APOE genotyping and genotype analysis was performed following standard procedures (Saykin *et al.*, 2010).

Neuropsychological assessment

Cognitive performance was assessed with a neuropsychological battery that covered a wide range of cognitive functions, including short and long-term memory, language, executive function and attention. We used baseline data from two composite scores, one for memory and one for executive function, derived from the ADNI neuropsychological battery that were recently validated using confirmatory factor analysis (Crane *et al.*, 2012; Gibbons, 2012). Specifically, the memory score integrated the Mini-mental state examination (MMSE), Rey Auditory Verbal Learning Test, Alzheimer's Disease Assessment Scale, and Logical Memory tests. The executive function score integrated the Category Fluency, Digit Span Backwards, Digit Symbol Substitution, Trails A and B and Clock Drawing tests.

ADNI Clinical Diagnosis

At the baseline visit, an initial diagnosis recommended by the ADNI Clinical Core was used to classify participants into Cognitively Normal (CDR=0, MMSE 24–30), Mild Cognitively Impaired (CDR=0.5, MMSE 24–30) and Alzheimer's disease (CDR 0.5-1, MMSE 20-26) (Aisen *et al.*, 2010, 2015; Petersen *et al.*, 2010).

CSF groups by neuropsychological status

To confirm that our CSF grouping strategy differentiated participants based on measures of neuropsychological status, we collapsed the baseline neuropsychological data from both ADNI cohorts to compare the aCSF and nCSF groups on the Mini Mental State Examination, a common test of general cognitive function, as well as the two composite scores of memory and executive function (see preceding section). For each test, we computed one way fixed effects ANOVAs with CSF group (aCSF, nCSF) as a factor, covarying for Age, Sex, Education, Cohort and APOE genotype. These models revealed significant main effects of CSF pathology on cognition in all tests. Consistent with the sensitivity of CSF pTau/Aβ to pathological aging, the aCSF group exhibited significantly more cognitive impairment than the nCSF group on Mini Mental State Examination, memory and executive function. See Table 1.

Table 1

Neuropsychological Function by CSF Group (collapsed across ADNI cohorts)

	CSF group			
	aCSF	nCSF	F	p
Mini Mental State Examination	26.28 (2.83)	28.65 (1.57)	$F_{1,830}=112.74$	$p<0.001$
Memory	-0.19 (0.81)	0.86 (0.68)	$F_{1,829}=243.77$	$p<0.001$
Executive Function	-0.20 (1.01)	0.72 (0.88)	$F_{1,829}=123.96$	$p<0.001$

Means and standard deviations of the neuropsychological tests. The aCSF group exhibited worse general cognition (MMSE), memory and executive function compared to the nCSF group. MMSE = Mini Mental State Examination; aCSF = abnormal CSF group; nCSF = normal CSF group.

Longitudinal structural MRI

A serial longitudinal pipeline scheme in SPM12 r7219 (https://www.fil.ion.ucl.ac.uk/spm/) implemented in Matlab 2013a was used to calculate the GM volume changes from the sMRI data (Ashburner and Ridgway, 2013). This procedure unifies rigid-body registration, intensity inhomogeneity correction and non-linear diffeomorphic transformation in a single iterative model. Initially, all of the individual time-points were co-registered to the ICBM 152 volume to ensure good starting parameters for the high-dimensional DARTEL warping algorithm. We then employed within-subject symmetric diffeomorphic registration of the two timepoints to create a midpoint average T1-image for each subject. Computing a mid-point average image prevents introduction of biases associated with using individual time-points as the reference (e.g., results differ depending of the time-point that is used as a reference). The mid-point average was scaled by the interscan interval. The registration step produced Jacobian determinant maps, which index contractions and expansions for each time-point relative to the mid-point average image. The default parameters for noise estimation, warping and bias regularizations were used. The mid-point average images were then segmented using SPM's unified segmentation (Ashburner and Friston, 2005) with the following settings: light regularization, 60mm of FWHM gaussian smoothness of bias and 2,2,2,3,4,2 Gaussians per tissue type. The resulting 1.5mm^3 GM and white matter maps were used to create separate DARTEL group templates for each sample (ADNI-1, and ADNI-GO/2). The DARTEL algorithm improves the inter-subject alignment by using multiple parameters per voxel when aligning the images (Ashburner, 2007). The segmented GM maps were multiplied by the Jacobian determinants of each time-point (Mechelli *et al.*, 2005). We then warped the segmented GM and white matter maps into the DARTEL template space with the 'preserve amount' option. Default settings were used elsewhere. The warping step produced modulated GM and white matter volumetric maps for each timepoint.

To check the quality of the images for subsequent analyses, the warped, modulated GM maps of each timepoint were visually inspected for segmentation and normalization inaccuracies by creating a plot showing a slice for all the subjects and were inspected for the presence of outliers by calculating the correlation between all the volumes using the CAT12 toolbox (http://dbm.neuro.uni-jena.de/cat/). Subjects that exhibited a correlation below 2 standard

deviations and abnormalities on their segmented GM volume (e.g. low signal intensity, inhomogeneities, warping errors) were excluded. Two subjects were discarded due to low data quality in ADNI-1 and eight in ADNI-GO/2. See Table 2 for complete information of the included participants.

Table 2

Participant Demographics, APOE Genotype and CSF assays

Profile	Dataset					
	ADNI-1			**ADNI-GO/2**		
	aCSF	nCSF	Test	aCSF	nCSF	Test
N (Total)	174	110	χ^2=14.42***	316	237	χ^2=11.28***
CN/MCI/AD	28/89/57	64/41/5	χ^2=64.26***	39/130/147	162/75/0	χ^2=230.84***
Age	74.51 (7.04)	75.53 (6.5)	*t*=-1.24	72.16 (7.22)	70.44 (6.56)	*t*=2.91**
Female/Male	66/108	50/60	χ^2=1.28	146/170	110/127	χ^2=0.00
Education	15.57 (2.99)	15.88 (2.89)	*t*=-0.87	15.96 (2.66)	16.62 (2.56)	*t*=2.96**
ε4+/ε4-	124/50	16/94	χ^2=84.48***	222/94	60/177	χ^2=107.54***
Aβ	579.28 (179.15)	1468.76 (554.28)	*t*=-16.30***	641.66 (192.73)	1376.54 (589.78)	t=-18.45***
pTau	34.33 (12.33)	19.6 (6.45)	*t*=13.16***	35.75 (14.98)	18.23 (6.52)	*t*=18.57***

Information of the included participants from the ADNI-1 and ADNI-GO/2 cohorts by CSF group. Values represent means (standard deviations) unless otherwise specified. aCSF = abnormal CSF group; nCSF = normal CSF group: Aβ = CSF concentration of the amyloid beta 1-42 peptide; pTau = CSF concentration of hyper phosphorylated tau (at threonine 181). Independent samples t-tests (t) and chi-square (χ^2) tests were used to test CSF group differences within each ADNI Cohort. Baseline clinical diagnosis: CN=cognitively normal, MCI=mild cognitively impaired, AD=Alzheimer's disease. APOE status: ε4+ = ε4 carrier, ε4- = ε4 non-carrier. Age and Education are in years. Aβ1-42 and pTau concentrations are in picograms per milliliter (pg/mL). ***p<0.001, **p<0.005.

ROI definition

To test the predictive pathological models between the NbM and EC, we extracted GM volumes from two regions of interest (ROIs) using probabilistic atlases. Bilateral anatomical ROIs were created in MNI space with the SPM Anatomy Toolbox r 2.2b (http://www.fz-juelich.de/inm/inm-1/DE/Forschung/_docs/SPMAnatomyToolbox/SPMAnatomyToolbox_node.html) using previously published probabilistic maps of the NbM (Zaborszky *et al.*, 2008) and the EC (Amunts *et al.*, 2005). The NbM ROI is equivalent to areas Ch4 and Ch4p (Mesulam, 1983; Mesulam and Geula, 1988). The ROIs were then resampled and warped to the DARTEL group template (see Fig. 1b). Estimates of modulated GM volume (in units of milliliters) at each time-point were obtained using the ROI as a masking region, and by summing the total intensity of voxels falling within the masking region adjusted for the size and number of voxels (http://www0.cs.ucl.ac.uk/staff/g.ridgway/vbm/get_totals.m). No spatial smoothing was applied to the volumes. In addition, the total gray matter (TGM) from the modulated and warped individual time points was calculated using the same procedure. The total intracranial volume (TICV) was computed by summing up the tissue volumes of GM, white matter and CSF of the segmented average images produced in a previous step using the *seg8.mat file from the segmentation (Malone *et al.*, 2015).

In order to assess longitudinal changes in GM volumes, annualized percent change (APC) from baseline was calculated with the following formula (Cavedo *et al.*, 2017):

$$APC = \left(\frac{changebaseline(mL)}{valuebaseline(mL)}\right) \times \left(\frac{365}{interscaninterval(days)}\right) \times 100$$

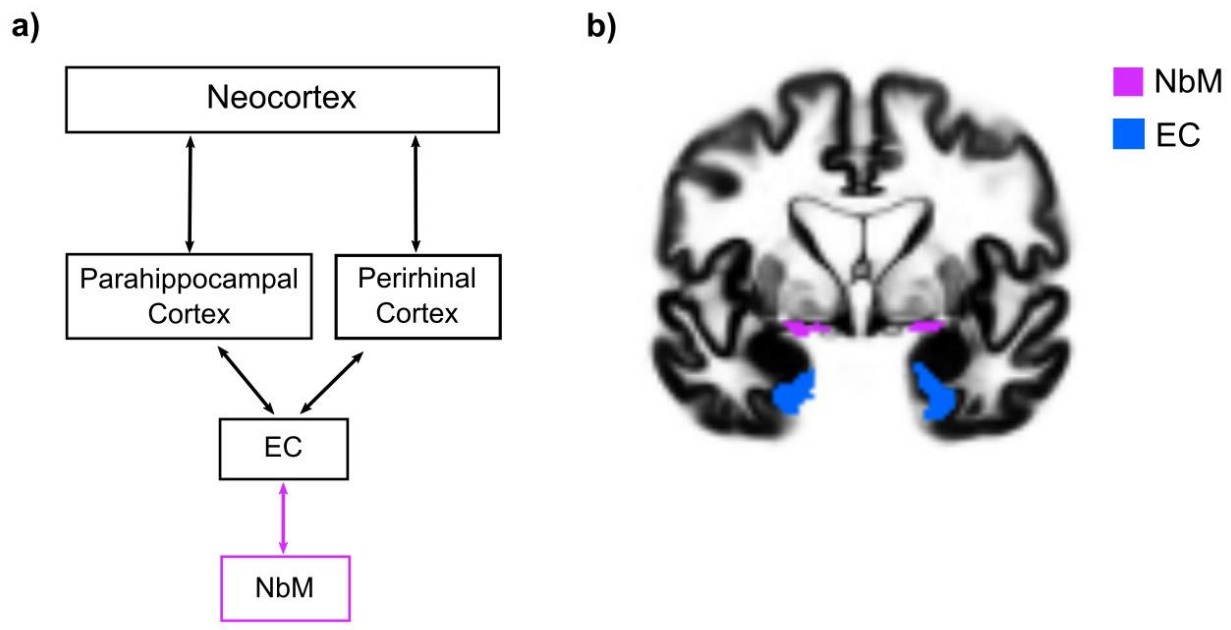

Figure 1. Proposed BF→entorhinal→neocortical model and regions of interest. (a) Predictive pathological staging model of tau pathology originating in EC and spreading via trans-synaptic mechanism to cortical targets of its projection system (black squares) updated to incorporate the BF degeneration as an 'upstream' event in the pathological cascade (purple square). (b) Regions of interest of the NbM (purple) and the EC (blue) are superimposed on a coronal slice of the population DARTEL template. Panel (a) is adapted with permission from (Liu *et al.*, 2012).

Statistical Analyses

ANOVA: To compare baseline volumes and longitudinal volume changes between the CSF groups, we computed fixed effects ANOVAs for each ADNI cohort and each ROI with CSF Group (aCSF, nCSF) as a factor covarying for Age, Sex, Education, TICV, baseline TGM and APOE genotype (see Supplementary Fig. 1 for the bivariate correlation values among the modeled variables). We then pooled the data from both ADNI Cohorts and computed one way fixed effects ANOVAs with CSF group (aCSF, nCSF) as a factor, correcting for the same covariates, and an additional covariate for study Cohort (Ma *et al.*, 2018). All ANOVA models were carried out in R with a type III sums of squares.

Robust regression: To test the predictive staging models (NbM→EC and EC→NbM), robust linear regression analyses were carried out in Matlab R2018b with *filtm* and a bisquare weight function to minimize the influence of outliers. Each model covaried for Age, Sex, Education, TICV, baseline TGM and APOE genotype. The predictive models were calculated first for each dataset separately and then in the pooled sample collapsing across both Cohorts and including and additional covariate for Cohort.

Moderation analyses of independent samples: The moderation analyses (Fig. 3e and 3j) were carried out using the PROCESS macro for SPSS (Hayes, 2012) retrieved from http://www.afhayes.com/public/process2012.pdf. 2012). The aCSF and nCSF groups served as the dichotomous moderator variable in all models. Age, Sex, Education, TICV, baseline TGM, APOE genotype and Cohort were included as covariates in all models. All data were mean centered. The moderation analysis employed a heteroscedasticity consistent standard error and covariance matrix estimator.

Comparison of correlations between dependent samples: To compare correlation coefficients between the NbM→EC and EC→NbM models, we used *cocor* to account for the dependence between the two models (Diedenhofen and Musch, 2015).

Whole-brain analysis

To investigate the anatomical specificity of the relationship between baseline NbM volumes and longitudinal degeneration in the EC, we pursued an exploratory whole brain voxel-wise analysis. Whole-brain APC maps were calculated with the previous APC formula with the *imcalc* tool in SPM12. The APC maps were smoothed with a 4mm FWHM Gaussian kernel (Grothe *et al.*, 2012; Cantero *et al.*, 2017). For exploratory purposes, we tested a model with baseline EC predicting APC in every voxel in the aCSF group pooled across the ADNI-1 and ADNI-GO/ADNI-2 datasets. These regression models were estimated with non-parametric permutation testing using the Statistical NonParametric Mapping toolbox v13 (http://warwick.ac.uk/snpm) for SPM12

(Nichols and Holmes, 2002). Age, Sex, Education, TICV, baseline TGM, APOE genotype and Cohort were included as covariates. The models were estimated with 5000 permutations, without variance smoothing and global normalization, and including an explicit mask of the binarized and thresholded (>0.1) DARTEL GM ADNI-GO/2 group template. Results are presented with a voxel-level threshold of $p<0.05$ Family-Wise Error (FWE) corrected for multiple comparisons across the brain.

Results

Abnormal CSF pTau/Aβ differentiates MRI indices of NbM and EC neurodegeneration

We first examined how the CSF pTau/Aβ grouping criteria differentiates patterns of baseline NbM and EC volume. Consistent with the sensitivity of CSF to neuropathology, we found that individuals with abnormal CSF cut-offs had smaller baseline volumes in the NbM in the ADNI-1 (main effect of CSF Group: $F_{1,276}=9.04$, $p=0.002$), ADNI-GO/2 (main effect of CSF Group: $F_{1,594}=78.16$, $p<0.001$) and in the pooled data of both cohorts (main effect of CSF Group: $F_{1,828}=75.88$, $p<0.001$; Fig 2a). Baseline volumes of the EC were also smaller in the aCSF group in ADNI-1 (main effect of CSF Group: $F_{1,276}=8.71$, $p=0.003$), ADNI-GO/2 (main effect of CSF Group: $F_{1,594}=21.98$, $p<0.001$) and in the pooled data (main effect of CSF Group: $F_{1,828}=25.86$, $p<0.001$; Fig 2b).

We next examined if the CSF pTau/Aβ grouping criteria influenced longitudinal indices of APC in the NbM and EC at each ADNI Cohort. These models revealed that individuals with abnormal CSF biomarkers showed more longitudinal atrophy in the NbM in the ADNI-GO/2 (main effect of CSF Group: $F_{1,594}=7.60$, $p=0.005$) and in the pooled dataset (main effect of CSF Group: $F_{1,828}=9.79$, $p=0.002$), but not in ADNI-1 (main effect of CSF Group: $F_{1,276}=2.54$, $p=0.11$; Fig 2c). In the EC, the aCSF group exhibited more longitudinal atrophy in ADNI-1 (main effect of CSF Group: $F_{1,276}=23.91$, $p<0.001$), ADNI-GO/2 (main effect of CSF Group: $F_{1,594}=29.54$, $p<0.001$) and in the pooled data (main effect of CSF Group: $F_{1,828}=47.51$, $p<0.001$; Fig 2d).

Finally, we investigated if the magnitude of longitudinal degeneration in the NbM and in the EC differed between individuals at different disease stages. For that, we cross-referenced the CSF groups with the ADNI baseline Clinical Diagnosis and found that, individuals with abnormal CSF biomarkers in all disease stages had increased degeneration in the NbM and the EC. Crucially, individuals in the preclinical disease stage (aCSF and normal cognition at baseline) showed greater magnitudes of degeneration in the NbM and the EC compared to the cognitively normal controls (nCSF and normal cognition at baseline). See Supplementary Fig. 2 and Supplementary Table 1. Consistent with our hypotheses, CSF biomarkers of abnormal pTau/Aβ accumulation in the central nervous system differentiated both baseline gray matter volume and longitudinal gray matter degeneration in the NbM and EC.

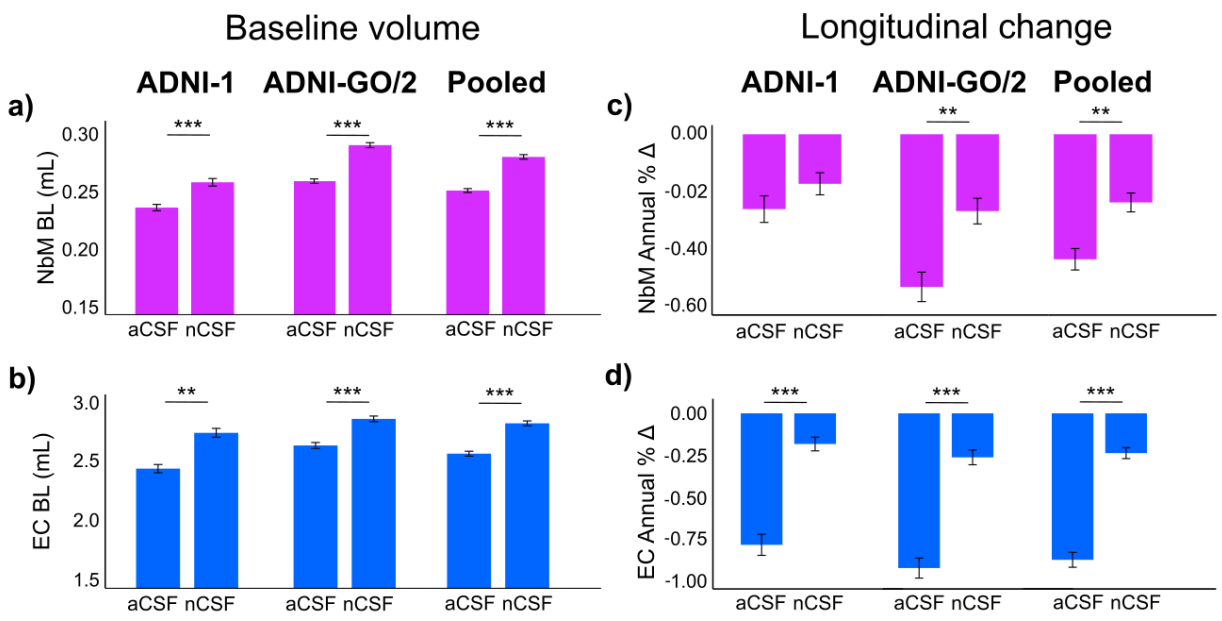

Figure 2. CSF biomarkers of neuropathology differentiate NbM and EC indices of structural degeneration. Bar plots showing the means and standard errors of the baseline and longitudinal changes of the NbM (purple bars) and EC (blue bars) a priori ROIs in the two independent datasets (ADNI-1 and ADNI-GO/2) and the pooled data of both datasets. Baseline NbM (a) and EC (b) volumes were smaller in the aCSF group. Longitudinal degeneration in the NbM (c) and in the EC (d) was larger in the aCSF group. aCSF=abnormal CSF group; nCSF=normal CSF group; NbM=nucleus basalis of Meynert, EC=entorhinal cortex. mL=milliliters, BL=baseline volume, asterisks denote statistical significance (***p<0.001; **p<0.01; *p<0.05).

Abnormal pTau/AB potentiates the predictive spread of NbM→EC degeneration

Thus far, our multimodal CSF and structural MRI analyses have treated patterns of neurodegeneration in the NbM and EC separately. We next used regression-based modelling to test if the degeneration in the NbM and in the EC reflects interdependent pathological processes. If degeneration in the NbM precedes degeneration in the EC due to selective neuronal vulnerability of cholinergic neurons inducing a 'spread' of pathology, then NbM baseline volumes should predict degeneration in the EC (NbM→EC). However, if degeneration in NbM and EC occurs in parallel due to a common global pathology, then baseline volumes of either region should predict degeneration in the other. Alternatively, if degeneration in NbM and EC reflects independent local pathology, then baseline volumes of neither region should predict degeneration in the other.

We used robust linear regression to examine these competing models in the aCSF and nCSF groups. Consistent with an interdependent NbM→EC model, we found in the aCSF group that baseline NbM volumes predicted longitudinal degeneration in the EC in both ADNI-1 (Fig. 3a; $r=0.20$, $t_{166}=2.12$, $p=0.03$) and ADNI-GO/2 (Fig. 3b; $r=0.37$, $t_{308}=5.15$, $p<0.001$). We next examined whether the predictive pathological staging of NbM and EC degeneration is observable under conditions of normal CSF pTau/Aβ. It could be the case that the underlying neuropathological process driving this relationship also occurs at 'neurotypical' levels of pTau/Aβ, but that this process is exacerbated in the aCSF group. In this case, we would expect to observe the same NbM→EC interrelationship, though possibly at a smaller magnitude. We found negligible evidence for the NbM→EC model in the nCSF group in ADNI-1 (Fig.3c; $r=-0.17$, $t_{102}=-1.14$, $p=0.25$). However, we did observe a predictive relationship in ADNI-GO/2 (Fig.3d, $r=0.21$, $t_{229}=2.47$, $p=0.01$). We then examined these relationships in the pooled data. The results supported the NbM→EC model in the aCSF ($r=0.30$, $t_{481}= 5.32$, $p<0.001$) but not the nCSF group ($r = 0.11$, $t_{338}=1.45$, $p=0.14$). See Figure 3e and Supplementary Table 2. To exclude the possibility that the results were distorted by possible collinearities among the model predictors and covariates, we computed each model without any of the covariates. The exclusion of covariates did not alter any of the above findings (see Supplementary Table 3). To directly test if the relationship observed in the pooled aCSF group was significantly different from the that observed in the pooled nCSF

group, we computed a moderation analysis with CSF group (aCSF, nCSF) as a dichotomous moderator on the NbM→EC interrelationship (see Methods). We found a significant moderating effect of CSF group on the NbM→EC interrelationship (t_{826}=2.55, p=0.01), indicating a more pronounced interregional spread in the aCSF compared to the nCSF group.

We next tested the competing model of EC→NbM predictive pathological spread, focusing first on the aCSF group. We found that EC baseline volumes did not predict longitudinal decreases in the NbM in ADNI-1 (Fig. 3f; r=-0.06, t_{166}=-0.56, p=0.57), in ADNI-GO/2 (Fig. 3g; r=0.10, t_{308}=1.18, p=0.23) or in the pooled sample (Fig.3j; r=0.02, t_{481}=0.26, p=0.79; Supplementary Table 1). Moreover, we found negligible evidence for the EC→NbM model in the nCSF group in ADNI-1 (Fig.3h; r=0.12, t_{102}=0.92, p=0.36), ADNI-GO/2 (Fig.3i, r=0.18, t_{229}=1.72, p=0.08), or in the pooled sample (Fig.3j; r=0.12, t_{334}=1.53 , p=0.12; Supplementary Table 1). Nor was there a significant interaction between CSF group and the relationship between EC and NbM in the pooled sample (Fig 3j; $t_{826=}$1, p=0.62).

We then directly compared the two predictive staging models, NbM→EC and EC→NbM, using a slopes analysis between dependent samples (see Methods). We found that the coefficients in each model were significantly different from one another in the aCSF group (z = 5.54; p<0.001; 95% r CI: 0.1831- 0.3847) but not in the nCSF group (z = 0.08; p=0.931; 95% r CI: -0.1424 - 0.13). See Figure 4.

Taken together, our predictive pathological models suggest that neurodegeneration of the cholinergic basal forebrain system may occur in both the aCSF and nCSF aging phenotypes, but that abnormal proteopathic pTau/Aβ accumulation greatly exacerbates this effect. The results also demonstrate that the EC→NbM model does not fit a neurobiologically plausible predictive staging of neurodegeneration in either the aCSF or nCSF cohort.

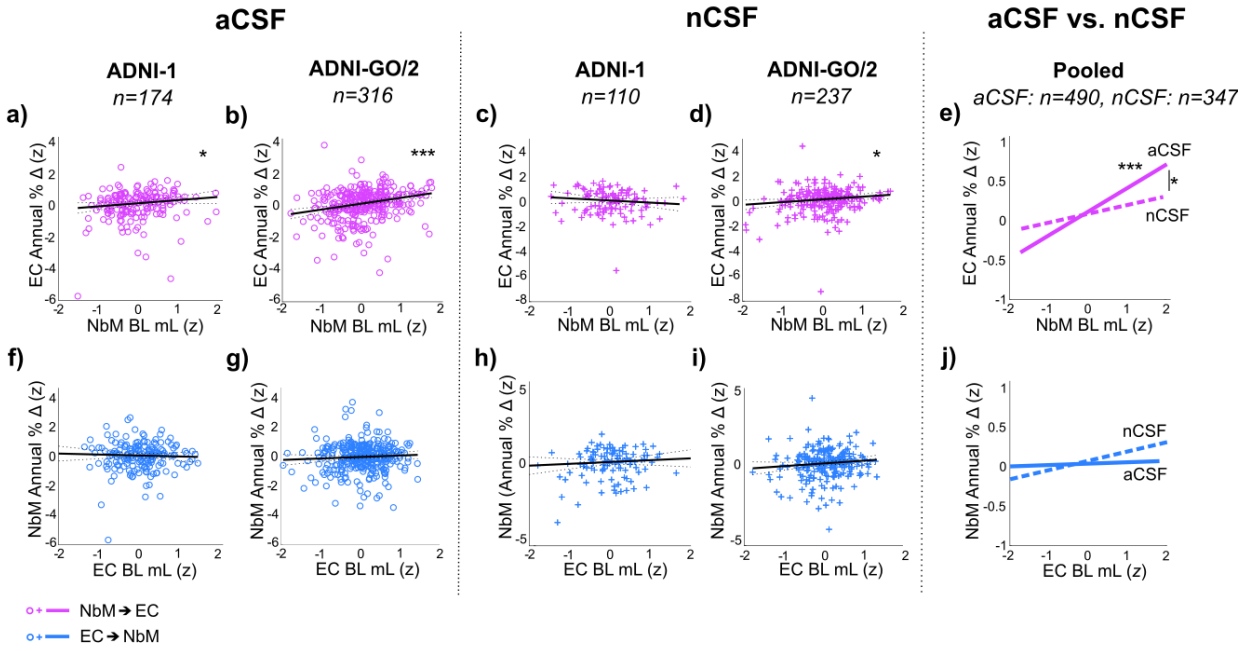

Figure 3. Predictive pathological staging models. In the aCSF group, smaller baseline NbM volumes (x-axis: negative z-score values) were associated with greater magnitudes of longitudinal degeneration in the EC (y-axis: negative z-score values for T2-T1 annual percent change) in both (a) ADNI-1 and (b) ADNI-GO/2 (lower left corner of the graphs). No such relationships were observed in the nCSF groups in (c) ADNI-1 but it was present in (d) ADNI-GO/2. (e) CSF concentrations of pTau/Aβ (nCSF versus aCSF) significantly moderated the relationship between baseline NbM volume and longitudinal EC degeneration. (f—j) Baseline EC volumes did not predict longitudinal degeneration in the NbM in either the aCSF or nCSF, in either ADNI-1 or ADNI-GO/2. Nor did it moderate this relationship. aCSF=abnormal CSF group; nCSF=normal CSF group; NbM=nucleus basalis of Meynert, EC=entorhinal cortex. mL=milliliters, BL=baseline volume, asterisks denote statistical significance (***p<0.001;*p<0.01; * p<0.05).

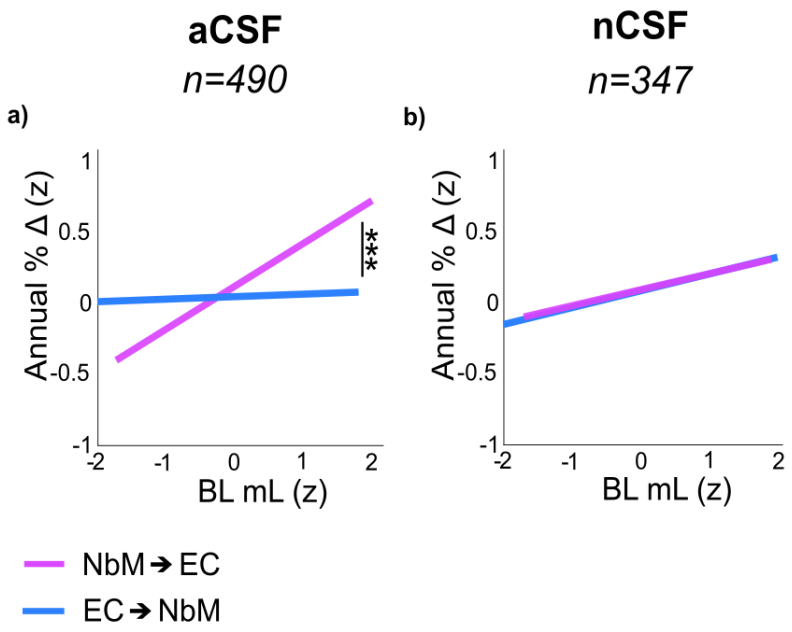

Figure 4. Aβ **and pTau potentiate the spread of neurodegeneration from NbM to EC.** The slopes of the NbM→EC and EC→NbM robust regression models were different in (a) the pooled aCSF group but (b) not in the pooled nCSF group. The x axes reflect baseline NbM volumes (purple lines) and baseline EC volumes (blue lines). The y axes reflect annual percent change in the EC (purple lines) and in the NbM (blue lines). Baseline volumes and annual percent change units were z-scored (z). aCSF=abnormal CSF group; nCSF=normal CSF group; NbM=nucleus basalis of Meynert, EC=entorhinal cortex. mL=milliliters, BL=baseline volume, asterisks denote statistical significance (***p<0.001;*p<0.01; * p<0.05).

Clinical diagnosis does not moderate the relationship between NbM→EC

Having demonstrated that the NbM→EC relationship was more prominent and reliable in the aCSF group, we then investigated whether the severity of the disease had an impact on the strength of this relationship in the pooled aCSF group. We expected that in initial (i.e. cognitively normal aCSF individuals) and advanced disease stages (i.e. cognitively impaired aCSF individuals), participants would show a weaker predictive relationship due to smaller magnitudes of EC atrophy in the early stages and reduced NbM atrophy in the more advanced stages (Schmitz and Spreng,

2016). Clinical diagnosis was not a significant moderating effect (Supplementary Figure 3; $t_{1,479}$=1.65, p=0.49), indicating that the predictive relationship was robust across clinical diagnostic subgroups of the aCSF cohort.

NbM→EC predictive pathological spreading is anatomically specific

How spatially selective is the observed interrelationship between NbM and EC in the aCSF group? To determine where degeneration is predicted based on NbM integrity, we performed a voxel-wise regression analysis between baseline volumes in the NbM and longitudinal APC in every brain voxel (see Methods). The model collapsed aCSF individuals across the two ADNI Cohorts into a single cohort. We found that baseline NbM volumes predicted degeneration in a circumscribed cluster of regions localized to the right entorhinal and perirhinal cortices and in the left middle temporal gyrus (Fig. 5a). The predictive pathological spread of NbM→EC neurodegeneration therefore exhibits a high degree of anatomical specificity.

In our a priori ROI-based regression models, we found negligible evidence in support of the EC→NbM model. However, following from non-human animal work (Khan *et al.*, 2014), we hypothesized that that predictive pathological spread of degeneration from EC might target anatomically and functionally connected cortical areas including the parahippocampal and posterior parietal cortices. To test this hypothesis, we computed a second voxel-wise regression analysis in the pooled aCSF group between baseline volumes in the EC and longitudinal APC in every brain voxel of the gray matter mask (see Methods). We found that baseline EC volumes predicted longitudinal degeneration in a circumscribed network of temporal cortical regions including the entorhinal, perirhinal, parahippocampal and fusiform cortices and temporal poles (Figure. 5b). Additional clusters were detected in the insular and posterior parietal cortices.

Finally, we tested the same models in the nCSF cohort, collapsing individuals from both ADNI Cohorts. No significant voxels were found at the corrected statistical threshold (p<0.05 FWE) in either of the models (NbM→whole brain; EC→whole brain). Taken together, the voxel-wise regression results show that among individuals expressing abnormal CSF: (1) baseline NbM volumes selectively predict degeneration in the EC and adjacent perirhinal cortex, and, (2) EC

degeneration 'spreads' to anatomically and functionally connected areas including the parahippocampal gyrus and other temporoparietal regions (Khan *et al.*, 2014).

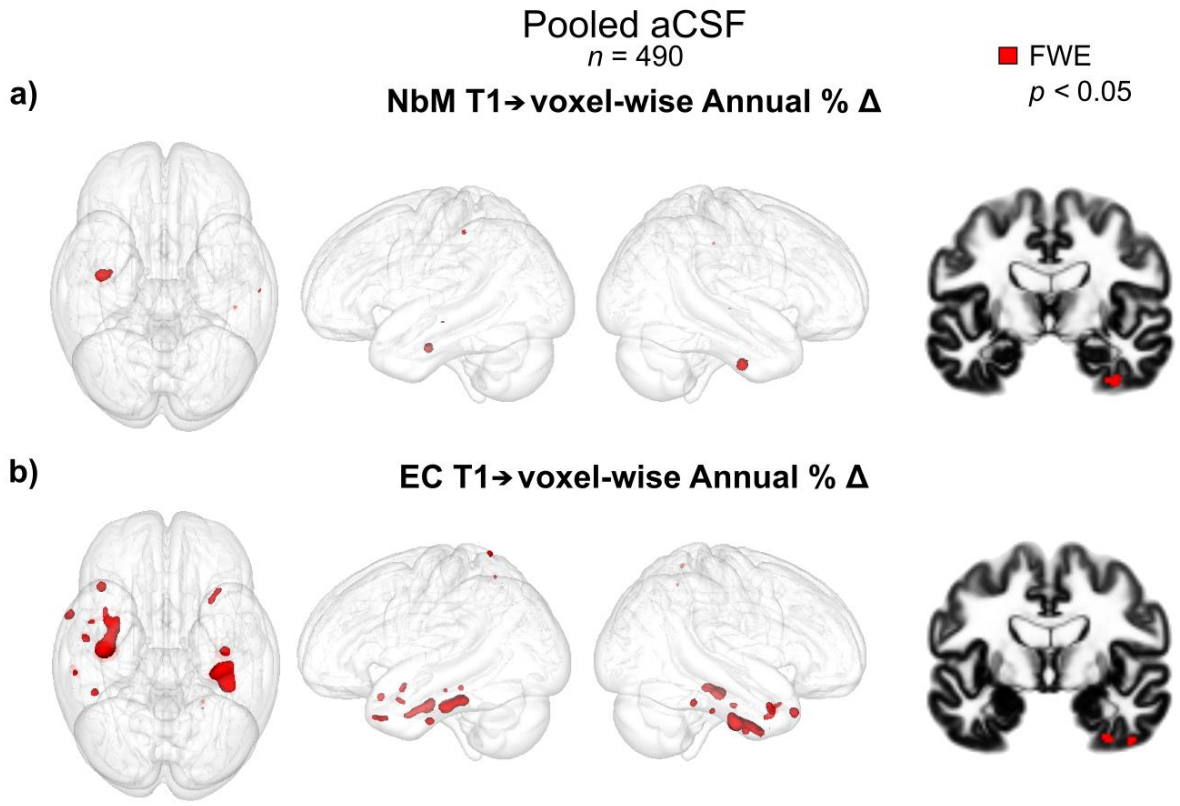

Figure 5. NbM and EC predict distinct patterns of downstream degenerative spreading. Baseline volumes of the NbM and the EC predicting APC in every brain voxel in the pooled aCSF group (n=490). In red, voxels showing a significant association with baseline volumes in the NbM (a) and in the EC (b) with a $p<0.05$ voxel-level FWE-corrected threshold. Baseline NbM volumes predicted degeneration in the EC whereas baseline EC volumes predicted degeneration in regions of the temporal and parietal cortices. Results are rendered into an MNI glass brain to the group DARTEL space using Mango (http://ric.uthscsa.edu/mango/). Models were tested for significance using non-parametric permutation testing. aCSF=abnormal CSF group; NbM=nucleus basalis of Meynert, EC=entorhinal cortex; FWE=Family-Wise Error.

Discussion

We provide evidence that degeneration in the NbM is an upstream event of subsequent degeneration in the EC and temporal cortices. Our results generalized across two non-overlapping and well-powered datasets. As hypothesized, the NbM→EC relationship was moderated by the presence of abnormal CSF biomarkers of pTau and Aβ, consistent with a mechanism of trans-synaptic spread of these proteins across anatomically connected regions. Using whole-brain regression models, we presented novel evidence that the relationship between baseline NbM volumes and neurodegeneration was spatially specific to regions of the EC and the perirhinal cortices, regions hypothesized to be among the earliest to be affected in Alzheimer's disease (Braak and Braak, 1991; Khan *et al.*, 2014). Finally, baseline EC volumes predicted neurodegeneration mainly in regions of the temporal cortex, recapitulating the prevailing staging model (Braak and Braak, 1991; Braak *et al.*, 2006; Liu *et al.*, 2012). These findings highlight the relevance of the cholinergic BF nuclei in Alzheimer's disease and motivate novel interventions targeted to these neuronal populations.

The intrinsic properties of the BF cholinergic neurons, including their location, connections and morphology, might be key to understanding why these cell types are selectively vulnerable in Alzheimer's disease (Mattson and Magnus, 2006). The NbM cholinergic neurons have large projecting axons with extensive arbors that expand long distances in the central nervous system (Wu *et al.*, 2014; Ballinger *et al.*, 2016). Extremely large axons and arbors exert high metabolic demands in order to support their maintenance, repair and transport. A less efficient cellular response to axonal perturbations could increase their vulnerability to the accumulation of abnormal proteins (Wu *et al.*, 2014). In addition, large surface areas increase their exposure to toxic environments (Mattson and Magnus, 2006). Consistent with its selective vulnerability, the NbM is one of the most vulnerable regions to the early accumulation of intracellular tau pathology (Mesulam *et al.*, 2004; Braak and Del Tredici, 2011) and, interestingly, intraneuronal amyloid oligomers (Baker-Nigh *et al.*, 2015). There is increasing evidence showing that intraneuronal amyloid can have deleterious early effects in the cells, such as disrupting their retrograde axonal transport machinery (Morfini *et al.*, 2009) which in turn can cause a neurotrophic deficiency

(Bellucci *et al.*, 2006) leading to neurodegeneration (De Lacalle *et al.*, 1996). *In vivo* structural MRI studies have added further support for the vulnerability of the BF, showing reduced BF volumes cross-sectionally (Grothe *et al.*, 2012; Cantero *et al.*, 2017) and longitudinally (Hall *et al.*, 2008; Grothe *et al.*, 2013; Schmitz *et al.*, 2018) in individuals in the Alzheimer's disease continuum.

In this study, the pathological spread of neurodegeneration from the NbM to the EC was exacerbated in individuals with abnormal levels of CSF pTau and Aβ. Evidence from non-human animal studies shows that protein aggregates can spread trans-synaptically to neuroanatomically connected regions. In an amyloid precursor protein mouse model of Alzheimer's disease, neuronal accumulation of Aβ was observed first in the EC, followed by the dentate gyrus, a downstream region receiving monosynaptic projections from the EC (Harris *et al.*, 2010). Evidence further suggests that tau aggregates propagate from the EC to limbic and then neocortical connected areas (De Calignon *et al.*, 2012; Kfoury *et al.*, 2012; Walker *et al.*, 2013; Wu *et al.*, 2016). For example, in mice that expressed human tau restricted to the EC, the axonal terminals of the EC projecting neurons showed increasing markers of tauopathy over time (Liu *et al.*, 2012). In all, this shows that Aβ and tau can propagate synaptically across neural networks of anatomically connected vulnerable cells. If the NbM is one of the earliest regions to accumulate tau and Aβ, then these proteins may spread to the EC trans-synaptically, inducing the observed downstream neurodegeneration. Our results are therefore compatible with animal research showing a trans-synaptic mechanism of abnormal spreading of tau proteins. However, to ultimately demonstrate that degeneration in the EC is driven by the spread of tau pathology from the NbM in humans, longitudinal studies integrating both structural MRI and tau positron emission tomography are needed. In addition, we observed a relationship between the NbM→EC in the normal CSF group. This effect was weaker and not reliable across samples, indicating the possibility that there are other age-related pressures on the NbM cholinergic neurons independent from Aβ and pTau (Nitsch *et al.*, 1992; Wurtman, 1992).

Using longitudinal whole-brain structural MRI, we also showed a reliable (Figure 3A—E) and highly specific (Figure 5A) sequence of neurodegeneration from the NbM to the EC. This result challenges the most widely accepted model of Alzheimer's disease staging, which posits that the neuropathological and neurodegenerative cascade initiates in the transentorhinal and EC (Braak and Braak, 1991; Corder *et al.*, 2000; Braak *et al.*, 2006; Liu *et al.*, 2012; Khan *et al.*, 2014). This model was primarily advanced from *post-mortem* histology studies that examined the brains of individuals who died at different ages from different causes, which showed tau aggregates forming in the EC even in non-demented individuals (Braak and Braak, 1991; Braak *et al.*, 2006). Predictive pathological staging based on histological strategies are limited by the heterogeneity of the post-mortem samples, the inability to track pathology with progressive neurodegeneration within individuals, the variability in tissue staining techniques used to profile underlying pathology, and the variability in anatomical coverage across both cortical and subcortical regions. We overcame these limitations by using an *in vivo* longitudinal neuroimaging strategy of predictive pathological staging in a large cohort of over 800 older adults. We quantified the baseline CSF profile of amyloid and tau pathology in each individual based on the automated Elecsys protocol, which was harmonized between samples. We then applied an independently defined cutpoint to delineate unbiased groups of individuals exhibiting abnormal and normal CSF biomarkers. By comparing the spreading dynamics of neurodegeneration between these two groups, we demonstrated that baseline NbM volumes predicted an accelerated annual rate of degeneration in a future time point in the EC in the presence of abnormally elevated Aβ and pTau. In addition, we found evidence that this neuropathological background was associated with neurodegenerative spreading from EC to targets of its projections in the medial temporal lobes. These latter findings parallel those of recent cross-species translational research comparing transgenic mouse models of Alzheimer's disease with at-risk human participants (Khan *et al.*, 2014). In all, our results added evidence that NbM degeneration is an earlier pathological event in the Alzheimer's disease pathological cascade.

Here, we showed that the NbM→EC model reliably generalized between two different populations. It is important to note that the data of the ADNI-GO/2 sample were acquired in 3T and the ADNI-1 in 1.5T scanners. Previous reports have only used 1.5 datasets (Schmitz and

Spreng, 2016) and it is well known that the signal to noise ratio of subcortical structures is higher at 3T (Tardif *et al.*, 2010; Marchewka *et al.*, 2014). It is therefore likely that degeneration in the NbM is more accurately quantified in the ADNI-GO/2 sample. Although it is estimated that approximately 90% of the NbM neurons in monkeys are cholinergic (Mesulam, 1983), to ultimately prove that the degeneration in the EC is driven by a cholinergic deficit in humans, degeneration that is specific to cholinergic cell types should be demonstrated. The combination of structural MRI with cholinergic positron emission tomography (Aghourian *et al.*, 2017; Schmitz *et al.*, 2018) could help elucidate this issue. Finally, late onset Alzheimer's disease is a complex, multifactorial (Veitch *et al.*, 2018), polygenic (Tan *et al.*, 2019) neurodegenerative disease. We found that the relationship between NbM→EC was robust to differences in APOE genotype and clinical diagnosis—the presence of Aβ and pTau was the most potent moderating factor observed in our study. Nevertheless, other inter-individual variables not modeled in the present study such as vascular health (Iturria-Medina *et al.*, 2016) could help gain additional insights on the selective vulnerability of the NbM and the EC to Alzheimer's disease.

In conclusion, the current study provides reliable and anatomically specific support for a predictive pathological staging model of Alzheimer's disease that progresses in the following sequence: NbM→EC→Neocortex. In all, our findings call into question the prevailing view of Alzheimer's disease pathogenesis, suggesting instead that degeneration of the basal forebrain cholinergic projection system is an upstream event to that of its most vulnerable cortical targets in the EC. If the cholinergic neurons of the BF are selectively vulnerable to the early accumulation and propagation of Alzheimer's disease pathology, then interventions targeting these neuronal populations in early disease stages may be useful for modifying disease progression prior to cognitive decline.

Acknowledgements

Data collection and sharing for this project was funded by the Alzheimer's Disease Neuroimaging Initiative (ADNI) (National Institutes of Health Grant U01 AG024904) and DOD ADNI (Department of Defense award number W81XWH-12-2-0012). ADNI is funded by the National Institute on Aging, the National Institute of Biomedical Imaging and Bioengineering, and through generous contributions from the following: AbbVie, Alzheimer's Association; Alzheimer's Drug Discovery Foundation; Araclon Biotech; BioClinica, Inc.; Biogen; Bristol-Myers Squibb Company; CereSpir, Inc.; Cogstate; Eisai Inc.; Elan Pharmaceuticals, Inc.; Eli Lilly and Company; EuroImmun; F. Hoffmann-La Roche Ltd and its affiliated company Genentech, Inc.; Fujirebio; GE Healthcare; IXICO Ltd.; Janssen Alzheimer Immunotherapy Research & Development, LLC.; Johnson & Johnson Pharmaceutical Research & Development LLC.; Lumosity; Lundbeck; Merck & Co., Inc.; Meso Scale Diagnostics, LLC.; NeuroRx Research; Neurotrack Technologies; Novartis Pharmaceuticals Corporation; Pfizer Inc.; Piramal Imaging; Servier; Takeda Pharmaceutical Company; and Transition Therapeutics. The Canadian Institutes of Health Research is providing funds to support ADNI clinical sites in Canada. Private sector contributions are facilitated by the Foundation for the National Institutes of Health (www.fnih.org). The grantee organization is the Northern California Institute for Research and Education, and the study is coordinated by the Alzheimer's Therapeutic Research Institute at the University of Southern California. ADNI data are disseminated by the Laboratory for Neuro Imaging at the University of Southern California. This work was supported in part by a grant from the NIA (R03 RAG060263A) (T.W.S. and R.N.S.) and the Canada First Research Excellence Fund (T.W.S. and R.N.S.). S.F.C was supported by the Doctoral College "Imaging the Mind" (FWF-W1233) of the Austrian Science Fund.

Disclosures

K.R.A.V.D. and J.A.G. are currently employed by Pfizer. This work was supported in part by a Pfizer Scientific Services Evaluation Agreement to R.N.S.

The authors declare no competing financial interests.

Supplementary material

CSF methods

CSF samples were frozen on dry ice within 1 hour after collection and shipped overnight on dry ice to the ADNI Biomarker Core laboratory at the University of Pennsylvania Medical Center. Aliquots (0.5mL) were prepared from these and stored in barcode-labeled polypropylene vials at –80º C. The RIDs of the participants with structural MRI data were merged with the *UPENNBIOMK9_04_19_17.csv* spreadsheet to obtain within-subjects indices of baseline CSF biomarker data. The Elecsys $A\beta_{1-4}$ protocol is currently under development and the performance beyond the upper technical limit (> 1700 pg/mL) has not been formally established. These values were provided by an extrapolation of the calibration curve and are restricted to research purposes and excluded for clinical decision making.

Rates of longitudinal degeneration by CSF groups and Clinical Diagnosis

To investigate whether the magnitude of longitudinal degeneration in the NbM and in the EC differed between healthy individuals and individuals at different disease stages, we cross-referenced the CSF groups (abnormal CSF = pTau/Aβ >= 0.028; normal CSF = pTau/Aβ <0.028) with the ADNI baseline clinical diagnosis. This yielded 5 groups of individuals: 1) CN: normal CSF and cognitively normal; 2) MCI/AD normal CSF: normal CSF and Mild Cognitive Impairment or AD; 3) PREC: abnormal CSF and cognitively normal; 3) PROD: abnormal CSF and Mild Cognitive Impairment and 5) AD; abnormal CSF and Alzheimer's disease. See

Supplementary Table 3. We then examined if the indices of longitudinal degeneration in the NbM and in the EC differed between the groups in the pooled sample (ADNI-1 and ADNI-GO/2; n=837) with a repeated-measures ANOVA covarying for Age, Gender, Education, TICV, baseline TGM, study Cohort and APOE genotype. We found a significant GROUP×ROI interaction ($F_{4,1665}$=12.94, p<0.001). In order to examine if the NbM and the EC dissociated at early disease stages, we focused the post-hoc comparison in the CN and the PREC groups. Independent sample t-tests revealed that the PREC group had larger magnitudes of degeneration in the NbM (t_{118}=2.27, p=0.025). However, and inconsistent with our previous report (Schmitz and Spreng, 2016), the magnitude of degeneration in the EC was also more pronounced in the PREC group than in the CN (t_{108}=2.70, p=0.007). In addition, we found a main effect of Group ($F_{4,1665}$=13.30, p<0.001) and ROI ($F_{4,1665}$=12.70, p<0.001). See Supplementary Fig. 2.

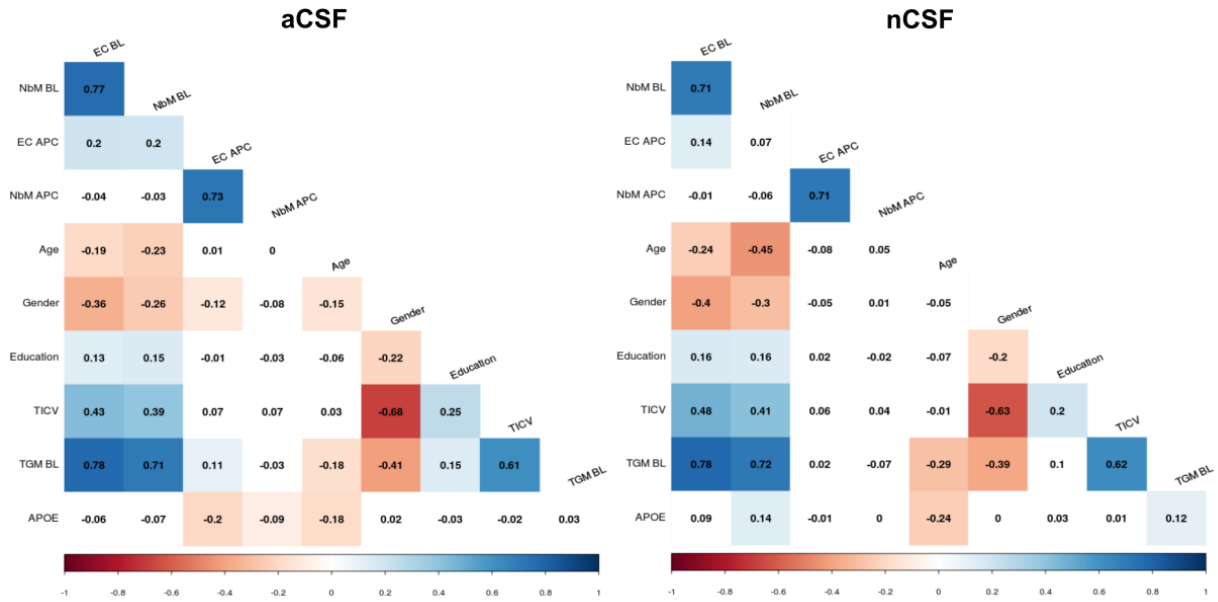

Supplementary Figure 1. Association between the variables included in the robust regression models. Pearson's correlation coefficients between the variables included in the robust regression models of the pooled (ADNI-1 and ADNI-GO/2) CSF groups. Note that the covariates (Age, Gender, Education, TICV and baseline TGM) are not statistically independent from the predictor variables (baseline volumes). Annual percent change (APC) volumes are the predicted variables

in all the models. Colored squares denote statistically significant correlations at $p<0.05$. aCSF=abnormal CSF group; nCSF=normal CSF group; NbM=nucleus basalis of Meynert; EC=entorhinal cortex; BL=Baseline; APC=annual percent change; TICV=total intracranial volume; TGM=total gray matter.

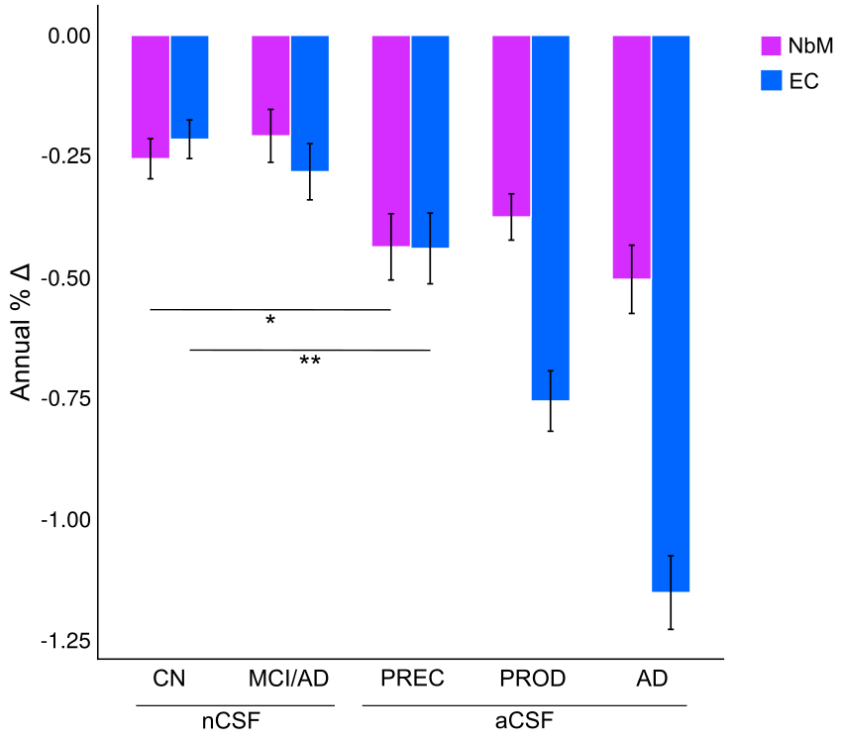

Supplementary Figure 2. GM degeneration according to CSF Group and Clinical Diagnosis. The magnitudes of longitudinal degeneration in the NbM and the EC differed between groups with different CSF status (normal vs. abnormal) and baseline clinical diagnosis. In the early disease stages (preclinical), NbM and EC degeneration was more pronounced than in the healthy control group (cognitively normal). CN=cognitively normal; MCI/AD=mild cognitively impaired or Alzheimer's disease; PREC=preclinical; PROD=prodromal; AD=Alzheimer's disease; aCSF=abnormal CSF group; nCSF=normal CSF group; NbM=nucleus basalis of Meynert; EC = entorhinal cortex.

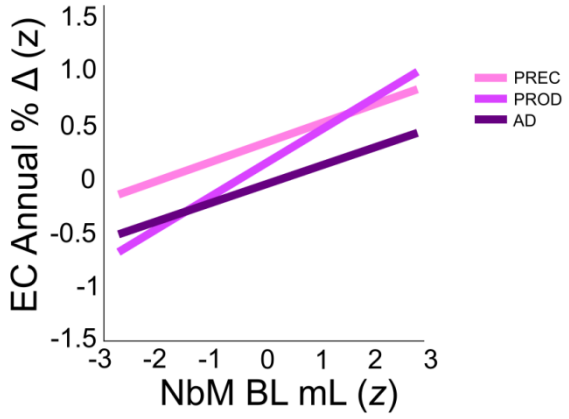

Supplementary Figure 3. Moderation of Clinical Diagnosis. The predictive relationship between baseline NbM and longitudinal degeneration in the EC was not moderated by the ADNI baseline Clinical Diagnosis (see main text). PREC=preclinical; PROD=prodromal; AD=Alzheimer's disease. The x axis reflects baseline NbM volumes and the y axis reflects annual percent change in the EC. Baseline volumes and annual percent change units were z-scored (z). NbM=nucleus basalis of Meynert; EC=entorhinal cortex; mL=milliliters; BL=baseline volume.

Supplementary Table 1

Participant Demographics by CSF Group and Baseline Clinical Diagnosis

	CSF group				
	nCSF		**aCSF**		
	CN	MCI/AD	PREC	PROD	AD
N	226	121	67	219	204
Age	71.74 (6.21)	72.63 (8.15)	74.97 (5.27)	72.88 (7.21)	72.46 (7.72)
Female/Male	118/108	42/79	38/29	85/134	89/115
Education	16.33 (2.64)	16.5 (2.77)	15.81 (2.82)	15.87 (2.92)	15.77 (2.62)
ε4+/ε4-	44/182	32/89	35/32	152/67	159/45
$A\beta_{1-42}$	1574.98 (579.71)	1089.76 (428.65)	643.99 (229.93)	630.99 (179.54)	599.14 (185.96)
pTau	19.47 (6.50)	17.16 (6.31)	29.41 (10.1)	35.14 (14.67)	37.28 (14.12)

Information of the included participants from the pooled (ADNI-1 and ADNI-GO/2) sample by CSF group and baseline Clinical Diagnosis. Values represent means (standard deviations) unless otherwise specified. aCSF=abnormal CSF group; nCSF=normal CSF group; CN=Cognitively Normal; PREC=preclinical; PROD=prodromal; AD=Alzheimer's Disease. Aβ=CSF

concentration of the amyloid beta 1-42 peptide; pTau=CSF concentration of hyper phosphorylated tau (at threonine 181). APOE status: ε4+ = ε4 carrier, ε4- = ε4 non-carrier. Age and Education are in years. Aβ1-42 and pTau concentrations are in picograms per milliliter (pg/mL). Values in parentheses are standard deviations.

Supplementary Table 2

Output of the Robust Regression Models in the Pooled (ADNI-1 and ADNI-GO/2) Sample

	CSF Group					
	aCSF (n=490)			**nCSF** (n=347)		
	NbM→EC			NbM→EC		
	Estimate	SE	t	Estimate	SE	t
Intercept	0.32	0.07	4.68***	0.09	0.05	1.87
Age	0.07	0.04	1.79	-0.09	0.05	-1.73
Female/Male	-0.05	0.05	-1.06	-0.02	0.06	-0.41
Education	-0.01	0.04	-0.23	0.02	0.05	0.53
TICV	-0.06	0.06	-1.00	0.06	0.07	0.88
TGM Baseline	-0.08	0.06	-1.27	-0.14	0.08	-1.77
Cohort	-0.13	0.04	-3.33***	-0.10	0.05	-1.92
ε4+/ε4-	-0.29	0.08	-3.56***	-0.04	0.11	-0.37
NbM Baseline	0.30	0.06	5.32***	0.11	0.08	1.45
	R-Squared: 0.103; F-statistic vs. constant model: 2.73, p-value = 0.0105			R-squared: 0.0366; F-statistic vs. constant model: 1.61, p-value = 0.122		

	EC→NbM			EC→NbM		
	Estimate	SE	t	Estimate	SE	t
Intercept	0.16	0.07	2.15**	0.08	0.05	1.52
Age	-0.03	0.04	-0.74	0.01	0.05	0.17
Female/Male	-0.08	0.06	-1.39	0.05	0.06	0.76
Education	-0.01	0.04	-0.16	0.02	0.05	0.33
TICV	0.04	0.06	0.61	0.14	0.07	1.96
TGM Baseline	-0.10	0.07	-1.42	-0.22	0.09	-2.46**
Cohort	-0.15	0.04	-3.74***	-0.05	0.05	-0.94
ε4+/ε4-	-0.17	0.09	-1.90	0.00	0.12	0.01
EC Baseline	0.02	0.07	0.26	0.12	0.08	1.53

	R-Squared: 0.052; F-statistic vs. constant model: 3.36, p-value = 0.000925	R-squared: 0.035; F-statistic vs. constant model: 1.53, p-value = 0.145

Estimated coefficients of the robust linear regression models in the pooled (ADNI-1 and ADNI-GO/2) sample. For each CSF group, two regression models were fitted (NbM→EC and EC→NbM). Values represent the estimated coefficients (Estimate), their standard errors (SE) and the associated t statistic (t) of the predictor variables. aCSF=abnormal CSF group; nCSF=normal CSF group; NbM=nucleus basalis of Meynert, EC=entorhinal cortex; TIVC=total intracranial volume; TGM=total gray matter; APOE status: ε4+ = ε4 carrier, ε4- = ε4 non-carrier. ***p<0.001, **p<0.005.

Supplementary Table 3

Robust Regression Models without Covariates

		CSF Group											
		aCSF						**nCSF**					
Dataset		NbM→EC			EC→NbM			NbM→EC			EC→NbM		
		Estimate	SE	t	Estimate	SE	t	Estimate	SE	t	Estimate	SE	t
ADNI-1	Intercept	0.13	0.05	2.35**	0.06	0.06	0.95	0.08	0.08	0.93	0.13	0.08	1.54
	Baseline Volume	0.19	0.05	3.43***	0.00	0.06	0.06	-0.00	0.08	-0.08	0.08	0.08	0.99
		R-squared=0.09; p<0.001			R-squared=0.00; p=0.34			R-squared=0.008; p=0.35			R-squared=0.03; p=0.06		
		NbM→EC			EC→NbM			NbM→EC			EC→NbM		
		Estimate	SE	t	Estimate	SE	t	Estimate	SE	t	Estimate	SE	t
ADNI-GO/2	Intercept	0.9	0.04	2.06**	0.02	0.04	0.53	0.08	0.05	1.76	0.08	0.5	1.47
	Baseline Volume	0.24	0.04	5.23***	0.00	0.04	0.03	0.09	0.05	1.90^{+}	-0.03	0.05	-0.63
		R-squared=0.09; p<0.001			R-squared=0.00; p=0.59			R-squared=0.03; p=0.01; $^{+}$p = 0.058			R-squared=0.01; p=0.11		
		NbM→EC			EC→NbM			NbM→EC			EC→NbM		
		Estimate	SE	t	Estimate	SE	t	Estimate	SE	t	Estimate	SE	t
Pooled	Intercept	0.13	0.03	3.71***	0.06	0.03	1.63	0.10	0.04	2.46**	0.08	0.04	2.01**
	Baseline Volume	0.18	0.03	5.15***	-0.04	0.03	-1.28	0.03	0.04	0.94	-0.01	0.044	-0.17
		R-squared=0.07; p<0.001			R-squared=0.00; p=0.03			R-squared=0.02; p=0.01			R-squared=0.01; p=0.04		

To ensure that our main findings were not distorted by collinearities in the model predictors, we re-estimated each model without the covariates for age, sex, education, TICV and baseline TGM. Baseline NbM volumes predicted longitudinal degeneration in the EC in all datasets. Values represent the estimated coefficients (Estimate), their standard errors (SE) and the associated t statistic (t) of the predictor variables. For each CSF group, two regression models were fitted (NbM→EC and EC→NbM). For the NbM→EC models, "Baseline Volume" refers to NbM. For the EC→NbM, "Baseline Volume" refers to EC. aCSF=abnormal CSF group; nCSF=normal CSF group; NbM=nucleus basalis of Meynert; EC=entorhinal cortex. ***$p<0.001$, **$p<0.005$.

Supplementary Table 4

Study Participants

RID	Cohort	pTau	$A\beta_{1-42}$	pTau/$A\beta_{1-42}$	CSF Group
*S_0003	ADNI1	22.83	741.5	0.031	aCSF
*S_0005	ADNI1	33.43	547.3	0.061	aCSF
*S_0010	ADNI1	31.26	357.4	0.087	aCSF
*S_0014	ADNI1	16.68	1582	0.011	nCSF
*S_0016	ADNI1	15.88	550.6	0.029	aCSF
*S_0022	ADNI1	21.85	2438	0.009	nCSF
*S_0023	ADNI1	16.74	1647	0.010	nCSF
*S_0029	ADNI1	27.24	442.9	0.062	aCSF
*S_0031	ADNI1	22.55	1774	0.013	nCSF
*S_0033	ADNI1	34.93	673	0.052	aCSF
*S_0040	ADNI1	12.5	1526	0.008	nCSF
*S_0041	ADNI1	18.07	414.6	0.044	aCSF
*S_0051	ADNI1	28.4	352.5	0.081	aCSF
*S_0057	ADNI1	30.25	597.1	0.051	aCSF
*S_0061	ADNI1	22.08	1288	0.017	nCSF
*S_0066	ADNI1	15.97	1477	0.011	nCSF
*S_0076	ADNI1	44.86	503.5	0.089	aCSF
*S_0077	ADNI1	65.4	792.7	0.083	aCSF
*S_0083	ADNI1	45.92	314.7	0.146	aCSF
*S_0084	ADNI1	29.85	479.6	0.062	aCSF
*S_0086	ADNI1	15.79	950.1	0.017	nCSF
*S_0089	ADNI1	14.88	1414	0.011	nCSF
*S_0091	ADNI1	30.16	502.6	0.060	aCSF
*S_0093	ADNI1	20.76	562.4	0.037	aCSF
*S_0094	ADNI1	36.96	462.4	0.080	aCSF
*S_0096	ADNI1	12.17	915.3	0.013	nCSF
*S_0097	ADNI1	18.06	776.6	0.023	nCSF
*S_0101	ADNI1	14.62	453.2	0.032	aCSF
*S_0102	ADNI1	27.85	539.3	0.052	aCSF
*S_0106	ADNI1	18.52	431.4	0.043	aCSF
*S_0107	ADNI1	16.31	1652	0.010	nCSF
*S_0112	ADNI1	24.43	498.6	0.049	aCSF
*S_0118	ADNI1	16.23	1467	0.011	nCSF
*S_0120	ADNI1	14.38	1226	0.012	nCSF
*S_0123	ADNI1	26.3	1566	0.017	nCSF
*S_0126	ADNI1	24.94	536.8	0.046	aCSF

*S_0127	ADNI1	30.66	2573	0.012	nCSF
*S_0129	ADNI1	26.45	682.7	0.039	aCSF
*S_0130	ADNI1	26.53	509.7	0.052	aCSF
*S_0139	ADNI1	45.14	651.9	0.069	aCSF
*S_0147	ADNI1	23.33	371.4	0.063	aCSF
*S_0149	ADNI1	19.07	652.1	0.029	aCSF
*S_0150	ADNI1	47.6	817	0.058	aCSF
*S_0158	ADNI1	21.69	2056	0.011	nCSF
*S_0159	ADNI1	9.74	622.7	0.016	nCSF
*S_0172	ADNI1	21.19	2070	0.010	nCSF
*S_0173	ADNI1	29.3	991.3	0.030	aCSF
*S_0176	ADNI1	40.9	670.7	0.061	aCSF
*S_0177	ADNI1	21.41	1367	0.016	nCSF
*S_0186	ADNI1	16.77	942.8	0.018	nCSF
*S_0196	ADNI1	16.32	540.6	0.030	aCSF
*S_0204	ADNI1	20.29	282.9	0.072	aCSF
*S_0210	ADNI1	18.54	1385	0.013	nCSF
*S_0214	ADNI1	48.14	683.1	0.070	aCSF
*S_0221	ADNI1	44.39	379.1	0.117	aCSF
*S_0222	ADNI1	31.9	620.3	0.051	aCSF
*S_0223	ADNI1	41.03	751.5	0.055	aCSF
*S_0231	ADNI1	31.15	426.1	0.073	aCSF
*S_0232	ADNI1	19.67	1028	0.019	nCSF
*S_0240	ADNI1	22.91	1338	0.017	nCSF
*S_0256	ADNI1	27.12	288.4	0.094	aCSF
*S_0257	ADNI1	21.4	427.2	0.050	aCSF
*S_0259	ADNI1	32.32	803.6	0.040	aCSF
*S_0260	ADNI1	15.47	1520	0.010	nCSF
*S_0269	ADNI1	32.75	576.8	0.057	aCSF
*S_0273	ADNI1	16.11	1639	0.010	nCSF
*S_0285	ADNI1	37.99	844.4	0.045	aCSF
*S_0286	ADNI1	40.28	642.9	0.063	aCSF
*S_0291	ADNI1	38.55	802.6	0.048	aCSF
*S_0292	ADNI1	13.1	941.7	0.014	nCSF
*S_0293	ADNI1	45.23	702.1	0.064	aCSF
*S_0294	ADNI1	24.75	2387	0.010	nCSF
*S_0295	ADNI1	34.73	888.1	0.039	aCSF
*S_0299	ADNI1	12.8	997.1	0.013	nCSF
*S_0300	ADNI1	32.87	475.2	0.069	aCSF
*S_0307	ADNI1	11.99	942.5	0.013	nCSF
*S_0314	ADNI1	32.43	379.7	0.085	aCSF

*S_0316	ADNI1	43.44	300.9	0.144	aCSF
*S_0326	ADNI1	24.04	1876	0.013	nCSF
*S_0327	ADNI1	16.71	1405	0.012	nCSF
*S_0331	ADNI1	39.86	588	0.068	aCSF
*S_0336	ADNI1	45.17	854.2	0.053	aCSF
*S_0341	ADNI1	19.33	313.1	0.062	aCSF
*S_0344	ADNI1	29.26	556.7	0.053	aCSF
*S_0352	ADNI1	15.45	1239	0.012	nCSF
*S_0361	ADNI1	38.22	585.5	0.065	aCSF
*S_0362	ADNI1	78.46	414.1	0.189	aCSF
*S_0366	ADNI1	30.61	508.9	0.060	aCSF
*S_0372	ADNI1	28.66	967	0.030	aCSF
*S_0374	ADNI1	24.03	495.2	0.049	aCSF
*S_0376	ADNI1	13.21	1148	0.012	nCSF
*S_0378	ADNI1	56.81	482.9	0.118	aCSF
*S_0386	ADNI1	16.77	1168	0.014	nCSF
*S_0388	ADNI1	31.59	332.6	0.095	aCSF
*S_0390	ADNI1	59.84	490	0.122	aCSF
*S_0394	ADNI1	33.87	643.4	0.053	aCSF
*S_0400	ADNI1	28.51	265.6	0.107	aCSF
*S_0403	ADNI1	36.23	333.5	0.109	aCSF
*S_0404	ADNI1	42.87	2401	0.018	nCSF
*S_0413	ADNI1	10.57	1006	0.011	nCSF
*S_0422	ADNI1	21.84	1907	0.011	nCSF
*S_0424	ADNI1	17.94	399.1	0.045	aCSF
*S_0426	ADNI1	14.3	374.5	0.038	aCSF
*S_0429	ADNI1	15.55	1014	0.015	nCSF
*S_0431	ADNI1	38.61	657.2	0.059	aCSF
*S_0433	ADNI1	24.9	831.3	0.030	aCSF
*S_0441	ADNI1	21.45	1614	0.013	nCSF
*S_0443	ADNI1	27.73	1850	0.015	nCSF
*S_0448	ADNI1	20.87	1645	0.013	nCSF
*S_0454	ADNI1	31.71	2108	0.015	nCSF
*S_0457	ADNI1	34.79	471.5	0.074	aCSF
*S_0459	ADNI1	27.12	2490	0.011	nCSF
*S_0464	ADNI1	14.12	1203	0.012	nCSF
*S_0467	ADNI1	23.98	500.5	0.048	aCSF
*S_0470	ADNI1	44.28	725.2	0.061	aCSF
*S_0472	ADNI1	20.22	1550	0.013	nCSF
*S_0474	ADNI1	41.6	441.2	0.094	aCSF
*S_0479	ADNI1	22.8	649.7	0.035	aCSF

*S_0481	ADNI1	35.95	594	0.061	aCSF
*S_0488	ADNI1	17.22	873.8	0.020	nCSF
*S_0498	ADNI1	19.71	2001	0.010	nCSF
*S_0507	ADNI1	31.48	449.8	0.070	aCSF
*S_0511	ADNI1	35.77	627.5	0.057	aCSF
*S_0514	ADNI1	10.41	826.8	0.013	nCSF
*S_0516	ADNI1	29.6	1860	0.016	nCSF
*S_0518	ADNI1	29.13	540.2	0.054	aCSF
*S_0519	ADNI1	15.07	1263	0.012	nCSF
*S_0520	ADNI1	20.72	600.2	0.035	aCSF
*S_0533	ADNI1	12.91	637.8	0.020	nCSF
*S_0534	ADNI1	12.95	806.8	0.016	nCSF
*S_0535	ADNI1	32.44	623	0.052	aCSF
*S_0543	ADNI1	44.35	663.7	0.067	aCSF
*S_0544	ADNI1	12.46	461.6	0.027	nCSF
*S_0547	ADNI1	32.4	2568	0.013	nCSF
*S_0552	ADNI1	39.15	648.4	0.060	aCSF
*S_0555	ADNI1	20.13	560.6	0.036	aCSF
*S_0559	ADNI1	15.82	1245	0.013	nCSF
*S_0565	ADNI1	27.29	212.3	0.129	aCSF
*S_0566	ADNI1	29.77	682.5	0.044	aCSF
*S_0567	ADNI1	20.69	368.6	0.056	aCSF
*S_0577	ADNI1	55.22	702.2	0.079	aCSF
*S_0578	ADNI1	27.56	585.6	0.047	aCSF
*S_0579	ADNI1	19.43	1429	0.014	nCSF
*S_0588	ADNI1	40.69	529.2	0.077	aCSF
*S_0602	ADNI1	16.98	1251	0.014	nCSF
*S_0604	ADNI1	30.47	1079	0.028	aCSF
*S_0605	ADNI1	23.7	1117	0.021	nCSF
*S_0607	ADNI1	39.89	507.3	0.079	aCSF
*S_0610	ADNI1	32.15	3187	0.010	nCSF
*S_0618	ADNI1	18.66	1323	0.014	nCSF
*S_0619	ADNI1	18.56	393.8	0.047	aCSF
*S_0621	ADNI1	42.85	467	0.092	aCSF
*S_0625	ADNI1	20.33	645.9	0.031	aCSF
*S_0626	ADNI1	36.67	644.9	0.057	aCSF
*S_0634	ADNI1	34.68	1770	0.020	nCSF
*S_0637	ADNI1	26.17	2594	0.010	nCSF
*S_0638	ADNI1	23.74	269.3	0.088	aCSF
*S_0644	ADNI1	16.04	338.4	0.047	aCSF
*S_0648	ADNI1	25.18	1479	0.017	nCSF

*S_0649	ADNI1	42.03	669.3	0.063	aCSF
*S_0657	ADNI1	15.06	1697	0.009	nCSF
*S_0658	ADNI1	35.69	488.5	0.073	aCSF
*S_0671	ADNI1	35.23	578.9	0.061	aCSF
*S_0672	ADNI1	19.13	1631	0.012	nCSF
*S_0673	ADNI1	62.83	455.1	0.138	aCSF
*S_0677	ADNI1	15.07	988.7	0.015	nCSF
*S_0680	ADNI1	19.69	1868	0.011	nCSF
*S_0685	ADNI1	22.82	2296	0.010	nCSF
*S_0686	ADNI1	13.56	657.6	0.021	nCSF
*S_0690	ADNI1	30.8	756.9	0.041	aCSF
*S_0692	ADNI1	8	390.9	0.020	nCSF
*S_0717	ADNI1	40.02	494.3	0.081	aCSF
*S_0722	ADNI1	24.96	1954	0.013	nCSF
*S_0723	ADNI1	18.02	692.3	0.026	nCSF
*S_0724	ADNI1	42.12	812.7	0.052	aCSF
*S_0725	ADNI1	21.53	566.7	0.038	aCSF
*S_0729	ADNI1	31.69	957.8	0.033	aCSF
*S_0731	ADNI1	27.56	744.2	0.037	aCSF
*S_0733	ADNI1	45.2	711.9	0.063	aCSF
*S_0739	ADNI1	39.06	1066	0.037	aCSF
*S_0746	ADNI1	22.1	1837	0.012	nCSF
*S_0748	ADNI1	16.76	520.8	0.032	aCSF
*S_0750	ADNI1	53.41	533.1	0.100	aCSF
*S_0753	ADNI1	32.08	547.6	0.059	aCSF
*S_0754	ADNI1	34.11	392.1	0.087	aCSF
*S_0768	ADNI1	18.85	404.3	0.047	aCSF
*S_0778	ADNI1	20.65	668.2	0.031	aCSF
*S_0779	ADNI1	28.19	742	0.038	aCSF
*S_0783	ADNI1	22.19	1038	0.021	nCSF
*S_0784	ADNI1	13.46	476.1	0.028	aCSF
*S_0796	ADNI1	13.11	1071	0.012	nCSF
*S_0800	ADNI1	22.75	565.2	0.040	aCSF
*S_0803	ADNI1	70.52	1147	0.061	aCSF
*S_0814	ADNI1	49.55	749.9	0.066	aCSF
*S_0818	ADNI1	18.7	1843	0.010	nCSF
*S_0834	ADNI1	33.9	524.4	0.065	aCSF
*S_0835	ADNI1	28.62	562.6	0.051	aCSF
*S_0839	ADNI1	44.42	730.1	0.061	aCSF
*S_0843	ADNI1	11.86	1298	0.009	nCSF
*S_0850	ADNI1	31.73	618.2	0.051	aCSF

*S_0861	ADNI1	30.85	371.4	0.083	aCSF
*S_0866	ADNI1	16.13	1271	0.013	nCSF
*S_0878	ADNI1	37.97	526.4	0.072	aCSF
*S_0886	ADNI1	17.65	1737	0.010	nCSF
*S_0891	ADNI1	22.49	680.8	0.033	aCSF
*S_0896	ADNI1	17.58	1208	0.015	nCSF
*S_0904	ADNI1	50.97	573.6	0.089	aCSF
*S_0906	ADNI1	32.63	908.9	0.036	aCSF
*S_0908	ADNI1	14.64	1314	0.011	nCSF
*S_0912	ADNI1	32.75	2079	0.016	nCSF
*S_0921	ADNI1	48.22	608.2	0.079	aCSF
*S_0923	ADNI1	20.83	1396	0.015	nCSF
*S_0925	ADNI1	12.15	602.8	0.020	nCSF
*S_0926	ADNI1	14.22	1351	0.011	nCSF
*S_0932	ADNI1	22.57	579.2	0.039	aCSF
*S_0941	ADNI1	28.06	755.1	0.037	aCSF
*S_0950	ADNI1	25.21	494	0.051	aCSF
*S_0952	ADNI1	19.45	385.4	0.050	aCSF
*S_0961	ADNI1	55.17	313.5	0.176	aCSF
*S_0972	ADNI1	46.32	696	0.067	aCSF
*S_0973	ADNI1	18.33	1604	0.011	nCSF
*S_0978	ADNI1	37.9	657.6	0.058	aCSF
*S_0981	ADNI1	34.13	1606	0.021	nCSF
*S_0984	ADNI1	36.02	200	0.180	aCSF
*S_0994	ADNI1	51.42	699.3	0.074	aCSF
*S_0997	ADNI1	40.44	944.8	0.043	aCSF
*S_1002	ADNI1	12.57	1449	0.009	nCSF
*S_1009	ADNI1	21.39	561.3	0.038	aCSF
*S_1010	ADNI1	27.78	594.9	0.047	aCSF
*S_1016	ADNI1	24.71	1044	0.024	nCSF
*S_1034	ADNI1	15.79	666.2	0.024	nCSF
*S_1035	ADNI1	34.21	935.3	0.037	aCSF
*S_1041	ADNI1	28.22	502.4	0.056	aCSF
*S_1045	ADNI1	19.72	2037	0.010	nCSF
*S_1046	ADNI1	17.92	732.9	0.024	nCSF
*S_1054	ADNI1	39.09	511.9	0.076	aCSF
*S_1063	ADNI1	28.29	685.5	0.041	aCSF
*S_1073	ADNI1	69.63	657.9	0.106	aCSF
*S_1081	ADNI1	37.49	596	0.063	aCSF
*S_1082	ADNI1	32.96	517.6	0.064	aCSF
*S_1097	ADNI1	50.89	775.6	0.066	aCSF

*S_1098	ADNI1	48.27	561.7	0.086	aCSF
*S_1109	ADNI1	32.4	449.2	0.072	aCSF
*S_1126	ADNI1	22.82	566.3	0.040	aCSF
*S_1130	ADNI1	56.14	664.3	0.085	aCSF
*S_1140	ADNI1	19.71	1735	0.011	nCSF
*S_1144	ADNI1	35.2	564.2	0.062	aCSF
*S_1168	ADNI1	19.88	915	0.022	nCSF
*S_1169	ADNI1	34.78	3357	0.010	nCSF
*S_1170	ADNI1	48.82	730.9	0.067	aCSF
*S_1171	ADNI1	15.13	511.1	0.030	aCSF
*S_1183	ADNI1	30.47	1583	0.019	nCSF
*S_1187	ADNI1	26.44	1714	0.015	nCSF
*S_1190	ADNI1	33.74	1880	0.018	nCSF
*S_1206	ADNI1	20.77	1979	0.010	nCSF
*S_1213	ADNI1	37.44	574	0.065	aCSF
*S_1217	ADNI1	23.8	912	0.026	nCSF
*S_1224	ADNI1	26.56	496.4	0.054	aCSF
*S_1227	ADNI1	18.66	1865	0.010	nCSF
*S_1246	ADNI1	54.61	723.1	0.076	aCSF
*S_1247	ADNI1	31.94	649.1	0.049	aCSF
*S_1250	ADNI1	16.84	1643	0.010	nCSF
*S_1260	ADNI1	16.07	1470	0.011	nCSF
*S_1262	ADNI1	50.13	529.5	0.095	aCSF
*S_1265	ADNI1	26.61	860.9	0.031	aCSF
*S_1268	ADNI1	14.62	545.1	0.027	nCSF
*S_1269	ADNI1	46.2	997.6	0.046	aCSF
*S_1281	ADNI1	38.49	350.9	0.110	aCSF
*S_1285	ADNI1	74.51	862.9	0.086	aCSF
*S_1293	ADNI1	20.8	291.1	0.071	aCSF
*S_1296	ADNI1	24.37	318.8	0.076	aCSF
*S_1309	ADNI1	32.46	570	0.057	aCSF
*S_1315	ADNI1	34.36	761.5	0.045	aCSF
*S_1318	ADNI1	13.63	1134	0.012	nCSF
*S_1321	ADNI1	13.99	1113	0.013	nCSF
*S_1341	ADNI1	33.26	507.1	0.066	aCSF
*S_1351	ADNI1	58.26	755.5	0.077	aCSF
*S_1352	ADNI1	21.45	1685	0.013	nCSF
*S_1371	ADNI1	39.73	538.9	0.074	aCSF
*S_1373	ADNI1	29.77	430.7	0.069	aCSF
*S_1379	ADNI1	24.47	1539	0.016	nCSF
*S_1394	ADNI1	24.9	391.2	0.064	aCSF

*S_1414	ADNI1	18.62	1308	0.014	nCSF
*S_1419	ADNI1	22.48	390.5	0.058	aCSF
*S_0166	ADNI2	24.16	551.9	0.044	aCSF
*S_0311	ADNI2	21.32	1396	0.015	nCSF
*S_0416	ADNI2	17.14	1219	0.014	nCSF
*S_0668	ADNI2	15.31	1129	0.014	nCSF
*S_1106	ADNI2	27.39	829	0.033	aCSF
*S_4001	ADNI2	26.31	294.7	0.089	aCSF
*S_4003	ADNI2	28.47	1274	0.022	nCSF
*S_4005	ADNI2	36.63	853.5	0.043	aCSF
*S_4007	ADNI2	23.42	662.5	0.035	aCSF
*S_4010	ADNI2	14.52	681.8	0.021	nCSF
*S_4012	ADNI2	28.5	1009	0.028	aCSF
*S_4014	ADNI2	30.92	443.5	0.070	aCSF
*S_4015	ADNI2	39.81	384.6	0.104	aCSF
*S_4018	ADNI2	22.26	1893	0.012	nCSF
*S_4020	ADNI2	24.15	2559	0.009	nCSF
*S_4021	ADNI2	8	690.2	0.012	nCSF
*S_4022	ADNI2	47.72	427.9	0.112	aCSF
*S_4024	ADNI2	67.97	934.2	0.073	aCSF
*S_4026	ADNI2	18.33	509.2	0.036	aCSF
*S_4028	ADNI2	23.95	1910	0.013	nCSF
*S_4029	ADNI2	25.32	1063	0.024	nCSF
*S_4030	ADNI2	32.41	767.3	0.042	aCSF
*S_4032	ADNI2	12.23	1192	0.010	nCSF
*S_4034	ADNI2	46.46	486.2	0.096	aCSF
*S_4035	ADNI2	44.09	623.4	0.071	aCSF
*S_4037	ADNI2	17.76	1809	0.010	nCSF
*S_4039	ADNI2	57.04	593.6	0.096	aCSF
*S_4042	ADNI2	32.93	633.1	0.052	aCSF
*S_4043	ADNI2	21.98	2232	0.010	nCSF
*S_4053	ADNI2	50.45	879	0.057	aCSF
*S_4057	ADNI2	56.96	950.8	0.060	aCSF
*S_4058	ADNI2	28.03	434.5	0.065	aCSF
*S_4059	ADNI2	20.2	374.4	0.054	aCSF
*S_4060	ADNI2	14.75	737.5	0.020	nCSF
*S_4067	ADNI2	15.53	396.6	0.039	aCSF
*S_4071	ADNI2	33.3	701.3	0.047	aCSF
*S_4073	ADNI2	15.34	836.7	0.018	nCSF
*S_4075	ADNI2	25.94	2093	0.012	nCSF
*S_4076	ADNI2	15.14	1939	0.008	nCSF

*S_4079	ADNI2	50.27	704.5	0.071	aCSF
*S_4080	ADNI2	28.08	950.6	0.030	aCSF
*S_4081	ADNI2	22.37	715.5	0.031	aCSF
*S_4082	ADNI2	22.53	1616	0.014	nCSF
*S_4084	ADNI2	20.67	2349	0.009	nCSF
*S_4089	ADNI2	57.63	751.8	0.077	aCSF
*S_4090	ADNI2	17.53	1687	0.010	nCSF
*S_4093	ADNI2	10.42	858.7	0.012	nCSF
*S_4096	ADNI2	20.04	267.2	0.075	aCSF
*S_4097	ADNI2	21.89	801.7	0.027	nCSF
*S_4100	ADNI2	28.58	889.9	0.032	aCSF
*S_4103	ADNI2	17.69	1432	0.012	nCSF
*S_4104	ADNI2	13.66	917.4	0.015	nCSF
*S_4105	ADNI2	11.29	974.3	0.012	nCSF
*S_4114	ADNI2	47.82	916.1	0.052	aCSF
*S_4119	ADNI2	30.31	1826	0.017	nCSF
*S_4120	ADNI2	30.52	666.1	0.046	aCSF
*S_4121	ADNI2	26.15	1345	0.019	nCSF
*S_4122	ADNI2	36.58	1002	0.037	aCSF
*S_4125	ADNI2	14.88	1685	0.009	nCSF
*S_4127	ADNI2	8.21	744.5	0.011	nCSF
*S_4128	ADNI2	22.98	879.1	0.026	nCSF
*S_4131	ADNI2	28.22	589.1	0.048	aCSF
*S_4134	ADNI2	31.45	836.8	0.038	aCSF
*S_4139	ADNI2	10.84	1415	0.008	nCSF
*S_4146	ADNI2	19.83	519.9	0.038	aCSF
*S_4148	ADNI2	15.01	1352	0.011	nCSF
*S_4149	ADNI2	18.54	958.3	0.019	nCSF
*S_4150	ADNI2	19.39	2118	0.009	nCSF
*S_4151	ADNI2	17.85	492.7	0.036	aCSF
*S_4153	ADNI2	42.01	519.2	0.081	aCSF
*S_4157	ADNI2	29.16	1079	0.027	nCSF
*S_4158	ADNI2	16.87	1644	0.010	nCSF
*S_4160	ADNI2	10.84	1035	0.010	nCSF
*S_4162	ADNI2	35.37	778.8	0.045	aCSF
*S_4164	ADNI2	19.89	2326	0.009	nCSF
*S_4167	ADNI2	29.43	645.3	0.046	aCSF
*S_4168	ADNI2	21.1	723.4	0.029	aCSF
*S_4170	ADNI2	17.37	1073	0.016	nCSF
*S_4171	ADNI2	55	765.6	0.072	aCSF
*S_4172	ADNI2	47.67	651.4	0.073	aCSF

*S_4173	ADNI2	13.03	1358	0.010	nCSF
*S_4174	ADNI2	26.77	734.6	0.036	aCSF
*S_4176	ADNI2	46.98	1156	0.041	aCSF
*S_4177	ADNI2	15.28	924.7	0.017	nCSF
*S_4179	ADNI2	20.71	301.5	0.069	aCSF
*S_4185	ADNI2	9.55	723.1	0.013	nCSF
*S_4187	ADNI2	18.85	963.7	0.020	nCSF
*S_4188	ADNI2	27.59	485.5	0.057	aCSF
*S_4189	ADNI2	33.9	545.2	0.062	aCSF
*S_4192	ADNI2	21.54	564.5	0.038	aCSF
*S_4195	ADNI2	55.81	433.9	0.129	aCSF
*S_4196	ADNI2	36.31	1400	0.026	nCSF
*S_4197	ADNI2	17.74	555.4	0.032	aCSF
*S_4198	ADNI2	19.27	712.2	0.027	nCSF
*S_4200	ADNI2	13.05	1544	0.008	nCSF
*S_4201	ADNI2	59.94	749.4	0.080	aCSF
*S_4205	ADNI2	27.46	992.5	0.028	nCSF
*S_4208	ADNI2	16.95	1823	0.009	nCSF
*S_4211	ADNI2	20.36	456	0.045	aCSF
*S_4213	ADNI2	18.85	1691	0.011	nCSF
*S_4214	ADNI2	9.39	879.9	0.011	nCSF
*S_4215	ADNI2	27.32	576.4	0.047	aCSF
*S_4219	ADNI2	10.16	908.7	0.011	nCSF
*S_4223	ADNI2	23.49	834.6	0.028	aCSF
*S_4224	ADNI2	15.43	1201	0.013	nCSF
*S_4225	ADNI2	38.07	713.7	0.053	aCSF
*S_4229	ADNI2	9.92	925	0.011	nCSF
*S_4232	ADNI2	17.1	682	0.025	nCSF
*S_4235	ADNI2	32.64	697.2	0.047	aCSF
*S_4240	ADNI2	27.73	337.5	0.082	aCSF
*S_4241	ADNI2	32.12	731.9	0.044	aCSF
*S_4243	ADNI2	36.35	1069	0.034	aCSF
*S_4244	ADNI2	12.16	654.3	0.019	nCSF
*S_4245	ADNI2	9.22	924.4	0.010	nCSF
*S_4250	ADNI2	43.93	757.1	0.058	aCSF
*S_4251	ADNI2	21.73	728.5	0.030	aCSF
*S_4252	ADNI2	32.08	556.4	0.058	aCSF
*S_4254	ADNI2	31.96	1194	0.027	nCSF
*S_4258	ADNI2	34.52	641.6	0.054	aCSF
*S_4259	ADNI2	17.37	469.5	0.037	aCSF
*S_4262	ADNI2	34.28	790.5	0.043	aCSF

*S_4263	ADNI2	41.11	669.3	0.061	aCSF
*S_4266	ADNI2	33.22	820.1	0.041	aCSF
*S_4269	ADNI2	17.48	1157	0.015	nCSF
*S_4270	ADNI2	19.03	479.7	0.040	aCSF
*S_4272	ADNI2	20.08	601.8	0.033	aCSF
*S_4274	ADNI2	13.63	893.6	0.015	nCSF
*S_4275	ADNI2	20.11	1775	0.011	nCSF
*S_4276	ADNI2	21.92	2335	0.009	nCSF
*S_4278	ADNI2	19.33	422.8	0.046	aCSF
*S_4279	ADNI2	29.37	2612	0.011	nCSF
*S_4287	ADNI2	46.13	737.1	0.063	aCSF
*S_4288	ADNI2	10.96	716.6	0.015	nCSF
*S_4290	ADNI2	30.12	510.8	0.059	aCSF
*S_4291	ADNI2	18.84	762	0.025	nCSF
*S_4292	ADNI2	19.56	1635	0.012	nCSF
*S_4294	ADNI2	30.02	535	0.056	aCSF
*S_4300	ADNI2	14.1	633	0.022	nCSF
*S_4301	ADNI2	10.88	1052	0.010	nCSF
*S_4302	ADNI2	31.98	948.3	0.034	aCSF
*S_4303	ADNI2	24.99	668.7	0.037	aCSF
*S_4308	ADNI2	20.34	2040	0.010	nCSF
*S_4310	ADNI2	11.45	659.3	0.017	nCSF
*S_4312	ADNI2	20.75	666.2	0.031	aCSF
*S_4313	ADNI2	14.48	1244	0.012	nCSF
*S_4320	ADNI2	22	979.7	0.022	nCSF
*S_4324	ADNI2	15.05	342.6	0.044	aCSF
*S_4331	ADNI2	12.78	992	0.013	nCSF
*S_4335	ADNI2	16.11	203	0.079	aCSF
*S_4337	ADNI2	9.9	998.6	0.010	nCSF
*S_4339	ADNI2	27.13	481.2	0.056	aCSF
*S_4340	ADNI2	15.4	1913	0.008	nCSF
*S_4343	ADNI2	53.38	695.5	0.077	aCSF
*S_4346	ADNI2	26.35	664.5	0.040	aCSF
*S_4348	ADNI2	18.37	798.6	0.023	nCSF
*S_4349	ADNI2	17.82	995.8	0.018	nCSF
*S_4350	ADNI2	18.8	1918	0.010	nCSF
*S_4351	ADNI2	24.86	703.7	0.035	aCSF
*S_4352	ADNI2	23.04	1882	0.012	nCSF
*S_4357	ADNI2	19.25	1332	0.014	nCSF
*S_4359	ADNI2	46.74	871.9	0.054	aCSF
*S_4363	ADNI2	36.15	682.1	0.053	aCSF

*S_4365	ADNI2	17.29	1264	0.014	nCSF
*S_4366	ADNI2	46.64	729.9	0.064	aCSF
*S_4367	ADNI2	20.11	938.8	0.021	nCSF
*S_4369	ADNI2	24.56	2249	0.011	nCSF
*S_4371	ADNI2	24.15	957.2	0.025	nCSF
*S_4376	ADNI2	23.97	2108	0.011	nCSF
*S_4382	ADNI2	32.3	3088	0.010	nCSF
*S_4384	ADNI2	9.86	867.5	0.011	nCSF
*S_4385	ADNI2	12.76	220.6	0.058	aCSF
*S_4386	ADNI2	48.1	1221	0.039	aCSF
*S_4387	ADNI2	21.77	1099	0.020	nCSF
*S_4388	ADNI2	16.55	874.3	0.019	nCSF
*S_4391	ADNI2	13.94	1731	0.008	nCSF
*S_4392	ADNI2	37.26	976.6	0.038	aCSF
*S_4393	ADNI2	30.8	2573	0.012	nCSF
*S_4394	ADNI2	14.77	1086	0.014	nCSF
*S_4395	ADNI2	11.81	982.1	0.012	nCSF
*S_4396	ADNI2	13.69	981.6	0.014	nCSF
*S_4399	ADNI2	19.62	1554	0.013	nCSF
*S_4401	ADNI2	32.26	1867	0.017	nCSF
*S_4402	ADNI2	46.42	456.8	0.102	aCSF
*S_4404	ADNI2	21.19	652	0.033	aCSF
*S_4405	ADNI2	44.5	633.8	0.070	aCSF
*S_4406	ADNI2	25.55	810.6	0.032	aCSF
*S_4408	ADNI2	28.72	611.9	0.047	aCSF
*S_4410	ADNI2	29.14	2019	0.014	nCSF
*S_4414	ADNI2	43.22	969.7	0.045	aCSF
*S_4415	ADNI2	92.08	389	0.237	aCSF
*S_4417	ADNI2	19.6	801.2	0.024	nCSF
*S_4420	ADNI2	32.22	795	0.041	aCSF
*S_4421	ADNI2	17.55	1955	0.009	nCSF
*S_4422	ADNI2	30.51	1373	0.022	nCSF
*S_4423	ADNI2	19.7	741	0.027	nCSF
*S_4424	ADNI2	14.6	752.9	0.019	nCSF
*S_4426	ADNI2	17.89	819.6	0.022	nCSF
*S_4427	ADNI2	20.73	1689	0.012	nCSF
*S_4428	ADNI2	16.67	1454	0.011	nCSF
*S_4429	ADNI2	25.29	2175	0.012	nCSF
*S_4430	ADNI2	54.28	590.5	0.092	aCSF
*S_4433	ADNI2	33.76	486.5	0.069	aCSF
*S_4438	ADNI2	17.4	627.4	0.028	nCSF

*S_4442	ADNI2	51.24	425.6	0.120	aCSF
*S_4444	ADNI2	25.37	971.6	0.026	nCSF
*S_4447	ADNI2	45.51	871	0.052	aCSF
*S_4448	ADNI2	26.82	2426	0.011	nCSF
*S_4449	ADNI2	17.99	957.1	0.019	nCSF
*S_4453	ADNI2	19.29	2069	0.009	nCSF
*S_4456	ADNI2	27.26	689.2	0.040	aCSF
*S_4458	ADNI2	51.53	651.3	0.079	aCSF
*S_4462	ADNI2	21.12	721.6	0.029	aCSF
*S_4464	ADNI2	17.47	840.8	0.021	nCSF
*S_4466	ADNI2	15.52	1061	0.015	nCSF
*S_4467	ADNI2	76.51	705.2	0.108	aCSF
*S_4469	ADNI2	34.16	3384	0.010	nCSF
*S_4473	ADNI2	40.95	998.8	0.041	aCSF
*S_4474	ADNI2	36.17	507.2	0.071	aCSF
*S_4477	ADNI2	33.6	651.4	0.052	aCSF
*S_4480	ADNI2	23.17	682.1	0.034	aCSF
*S_4482	ADNI2	59.99	1244	0.048	aCSF
*S_4483	ADNI2	15.26	1696	0.009	nCSF
*S_4485	ADNI2	25.67	1563	0.016	nCSF
*S_4488	ADNI2	16.28	1641	0.010	nCSF
*S_4491	ADNI2	14.19	1292	0.011	nCSF
*S_4494	ADNI2	46.73	308.5	0.151	aCSF
*S_4496	ADNI2	28.25	3462	0.008	nCSF
*S_4498	ADNI2	35.75	876.6	0.041	aCSF
*S_4499	ADNI2	26.29	1841	0.014	nCSF
*S_4500	ADNI2	37.41	510.7	0.073	aCSF
*S_4501	ADNI2	31.57	741.5	0.043	aCSF
*S_4502	ADNI2	60.23	799.3	0.075	aCSF
*S_4503	ADNI2	17.1	1245	0.014	nCSF
*S_4505	ADNI2	28.49	2385	0.012	nCSF
*S_4507	ADNI2	30.48	697.3	0.044	aCSF
*S_4508	ADNI2	17.34	685.5	0.025	nCSF
*S_4510	ADNI2	47.52	733	0.065	aCSF
*S_4513	ADNI2	15.28	1085	0.014	nCSF
*S_4515	ADNI2	32.49	520.3	0.062	aCSF
*S_4516	ADNI2	19.91	1488	0.013	nCSF
*S_4520	ADNI2	35.59	2608	0.014	nCSF
*S_4521	ADNI2	50.4	918.5	0.055	aCSF
*S_4522	ADNI2	10.76	1084	0.010	nCSF
*S_4526	ADNI2	49.71	366	0.136	aCSF

*S_4530	ADNI2	19.88	592.3	0.034	aCSF
*S_4531	ADNI2	19.32	464.8	0.042	aCSF
*S_4538	ADNI2	28.11	761	0.037	aCSF
*S_4539	ADNI2	11.13	1093	0.010	nCSF
*S_4542	ADNI2	36.12	479.4	0.075	aCSF
*S_4545	ADNI2	11.89	1373	0.009	nCSF
*S_4546	ADNI2	24.81	523.9	0.047	aCSF
*S_4547	ADNI2	23.21	695.1	0.033	aCSF
*S_4549	ADNI2	32.02	531.8	0.060	aCSF
*S_4552	ADNI2	19.97	1241	0.016	nCSF
*S_4559	ADNI2	17.06	1969	0.009	nCSF
*S_4560	ADNI2	18.98	2140	0.009	nCSF
*S_4562	ADNI2	23.97	312.4	0.077	aCSF
*S_4565	ADNI2	16.72	495.8	0.034	aCSF
*S_4568	ADNI2	54.7	590.9	0.093	aCSF
*S_4576	ADNI2	55.14	2254	0.024	nCSF
*S_4577	ADNI2	12.84	318.3	0.040	aCSF
*S_4578	ADNI2	14.28	2054	0.007	nCSF
*S_4580	ADNI2	25.42	857	0.030	aCSF
*S_4582	ADNI2	33.56	786.9	0.043	aCSF
*S_4584	ADNI2	32.75	806	0.041	aCSF
*S_4585	ADNI2	18.76	1435	0.013	nCSF
*S_4586	ADNI2	19.26	1744	0.011	nCSF
*S_4587	ADNI2	24.38	686.4	0.036	aCSF
*S_4589	ADNI2	24.39	805.3	0.030	aCSF
*S_4591	ADNI2	28.67	651	0.044	aCSF
*S_4595	ADNI2	53	957.2	0.055	aCSF
*S_4596	ADNI2	23.72	473.8	0.050	aCSF
*S_4597	ADNI2	27.88	715.5	0.039	aCSF
*S_4598	ADNI2	29.77	2696	0.011	nCSF
*S_4599	ADNI2	15.8	772.8	0.020	nCSF
*S_4604	ADNI2	14.03	1279	0.011	nCSF
*S_4605	ADNI2	28.01	817.7	0.034	aCSF
*S_4611	ADNI2	20.44	574.2	0.036	aCSF
*S_4612	ADNI2	13.89	499.5	0.028	nCSF
*S_4615	ADNI2	30.62	864.5	0.035	aCSF
*S_4616	ADNI2	20.49	897.8	0.023	nCSF
*S_4621	ADNI2	14.55	853.3	0.017	nCSF
*S_4623	ADNI2	20.08	635.2	0.032	aCSF
*S_4624	ADNI2	37.45	608.9	0.062	aCSF
*S_4625	ADNI2	36.69	366.3	0.100	aCSF

*S_4629	ADNI2	10.33	1088	0.009	nCSF
*S_4631	ADNI2	30.41	725.4	0.042	aCSF
*S_4635	ADNI2	20.45	359.3	0.057	aCSF
*S_4636	ADNI2	30.4	744.4	0.041	aCSF
*S_4637	ADNI2	19.09	351.4	0.054	aCSF
*S_4638	ADNI2	15.52	1739	0.009	nCSF
*S_4641	ADNI2	21.43	660.7	0.032	aCSF
*S_4643	ADNI2	16.16	1704	0.009	nCSF
*S_4644	ADNI2	17.36	1778	0.010	nCSF
*S_4645	ADNI2	21.56	539.1	0.040	aCSF
*S_4657	ADNI2	59.14	883.8	0.067	aCSF
*S_4659	ADNI2	27.55	667.9	0.041	aCSF
*S_4660	ADNI2	62.39	767.6	0.081	aCSF
*S_4661	ADNI2	33.6	604	0.056	aCSF
*S_4668	ADNI2	33.14	698.1	0.047	aCSF
*S_4672	ADNI2	33.17	447.8	0.074	aCSF
*S_4674	ADNI2	31.89	843.1	0.038	aCSF
*S_4675	ADNI2	52.77	733.7	0.072	aCSF
*S_4679	ADNI2	31.59	1046	0.030	aCSF
*S_4680	ADNI2	24.13	487.9	0.049	aCSF
*S_4686	ADNI2	36.78	769.7	0.048	aCSF
*S_4688	ADNI2	31.12	1003	0.031	aCSF
*S_4689	ADNI2	32.4	747.3	0.043	aCSF
*S_4696	ADNI2	46.11	541.8	0.085	aCSF
*S_4707	ADNI2	17.93	451.7	0.040	aCSF
*S_4713	ADNI2	26.7	954.8	0.028	nCSF
*S_4714	ADNI2	36.67	915.7	0.040	aCSF
*S_4715	ADNI2	64.5	1009	0.064	aCSF
*S_4718	ADNI2	29.81	411.7	0.072	aCSF
*S_4720	ADNI2	31.28	483.9	0.065	aCSF
*S_4721	ADNI2	15.52	746.4	0.021	nCSF
*S_4728	ADNI2	31.27	507	0.062	aCSF
*S_4729	ADNI2	74.27	748.8	0.099	aCSF
*S_4730	ADNI2	24.06	588.2	0.041	aCSF
*S_4732	ADNI2	38.42	402.4	0.095	aCSF
*S_4736	ADNI2	28.48	440.3	0.065	aCSF
*S_4739	ADNI2	14.68	1404	0.010	nCSF
*S_4742	ADNI2	8.94	852.7	0.010	nCSF
*S_4743	ADNI2	22.83	844.8	0.027	nCSF
*S_4744	ADNI2	57.71	617.8	0.093	aCSF
*S_4746	ADNI2	20.32	880.2	0.023	nCSF

*S_4756	ADNI2	27.12	675.3	0.040	aCSF
*S_4757	ADNI2	59.81	701.5	0.085	aCSF
*S_4762	ADNI2	9.56	1020	0.009	nCSF
*S_4764	ADNI2	27.57	912.4	0.030	aCSF
*S_4765	ADNI2	50.75	845.8	0.060	aCSF
*S_4767	ADNI2	17.02	822.1	0.021	nCSF
*S_4770	ADNI2	24.93	503.1	0.050	aCSF
*S_4774	ADNI2	71.75	877.3	0.082	aCSF
*S_4782	ADNI2	20.02	312.3	0.064	aCSF
*S_4783	ADNI2	22.07	596.3	0.037	aCSF
*S_4793	ADNI2	30.19	443.9	0.068	aCSF
*S_4795	ADNI2	9.91	978.2	0.010	nCSF
*S_4796	ADNI2	74.45	755.2	0.099	aCSF
*S_4799	ADNI2	21.53	779.1	0.028	nCSF
*S_4801	ADNI2	26.96	375.7	0.072	aCSF
*S_4802	ADNI2	39.39	687.3	0.057	aCSF
*S_4804	ADNI2	14.99	432.8	0.035	aCSF
*S_4805	ADNI2	46	925	0.050	aCSF
*S_4806	ADNI2	8.87	927.5	0.010	nCSF
*S_4807	ADNI2	86.51	991.8	0.087	aCSF
*S_4809	ADNI2	26.79	782.6	0.034	aCSF
*S_4815	ADNI2	60.12	781.3	0.077	aCSF
*S_4816	ADNI2	52.08	511.3	0.102	aCSF
*S_4817	ADNI2	11.94	600.2	0.020	nCSF
*S_4820	ADNI2	64.84	384.4	0.169	aCSF
*S_4832	ADNI2	12.92	1236	0.010	nCSF
*S_4835	ADNI2	26.62	728.6	0.037	aCSF
*S_4845	ADNI2	38.18	652.1	0.059	aCSF
*S_4849	ADNI2	26.9	691.3	0.039	aCSF
*S_4852	ADNI2	58.19	685.7	0.085	aCSF
*S_4853	ADNI2	83.3	691.9	0.120	aCSF
*S_4855	ADNI2	21.48	732.8	0.029	aCSF
*S_4856	ADNI2	10.01	975.8	0.010	nCSF
*S_4857	ADNI2	36.33	888.5	0.041	aCSF
*S_4858	ADNI2	42.25	662.4	0.064	aCSF
*S_4863	ADNI2	32.73	449.4	0.073	aCSF
*S_4867	ADNI2	37.72	624.1	0.060	aCSF
*S_4868	ADNI2	30.84	519.7	0.059	aCSF
*S_4877	ADNI2	34.33	534.4	0.064	aCSF
*S_4878	ADNI2	14.75	1768	0.008	nCSF
*S_4879	ADNI2	37.91	532.9	0.071	aCSF

*S_4885	ADNI2	56.81	408.4	0.139	aCSF
*S_4888	ADNI2	31	876.8	0.035	aCSF
*S_4889	ADNI2	9.84	956.2	0.010	nCSF
*S_4891	ADNI2	25.35	533.5	0.048	aCSF
*S_4893	ADNI2	39.87	784.3	0.051	aCSF
*S_4894	ADNI2	47.59	423.6	0.112	aCSF
*S_4897	ADNI2	18.42	837.7	0.022	nCSF
*S_4898	ADNI2	16.42	711.2	0.023	nCSF
*S_4900	ADNI2	14.92	1605	0.009	nCSF
*S_4902	ADNI2	29.74	818.6	0.036	aCSF
*S_4903	ADNI2	27.5	854.8	0.032	aCSF
*S_4904	ADNI2	24.16	646.7	0.037	aCSF
*S_4905	ADNI2	46.04	568.8	0.081	aCSF
*S_4910	ADNI2	29.25	749.9	0.039	aCSF
*S_4911	ADNI2	17.17	330.9	0.052	aCSF
*S_4918	ADNI2	44.3	584.2	0.076	aCSF
*S_4919	ADNI2	17.85	989.8	0.018	nCSF
*S_4920	ADNI2	19.81	597.7	0.033	aCSF
*S_4921	ADNI2	11.77	1291	0.009	nCSF
*S_4925	ADNI2	27.16	694	0.039	aCSF
*S_4926	ADNI2	10.46	799.5	0.013	nCSF
*S_4928	ADNI2	33.02	883.9	0.037	aCSF
*S_4929	ADNI2	45.24	563.2	0.080	aCSF
*S_4936	ADNI2	18.52	518.3	0.036	aCSF
*S_4938	ADNI2	25.04	664.4	0.038	aCSF
*S_4940	ADNI2	30.36	652	0.047	aCSF
*S_4944	ADNI2	19.22	664.8	0.029	aCSF
*S_4945	ADNI2	28.27	757	0.037	aCSF
*S_4947	ADNI2	31.48	574.7	0.055	aCSF
*S_4949	ADNI2	36.03	506.1	0.071	aCSF
*S_4951	ADNI2	12.12	1024	0.012	nCSF
*S_4952	ADNI2	17.18	2429	0.007	nCSF
*S_4954	ADNI2	24.52	816.4	0.030	aCSF
*S_4955	ADNI2	13.28	395	0.034	aCSF
*S_4959	ADNI2	19.02	349.8	0.054	aCSF
*S_4962	ADNI2	47.15	998.2	0.047	aCSF
*S_4964	ADNI2	39.35	549.7	0.072	aCSF
*S_4971	ADNI2	28.66	471.3	0.061	aCSF
*S_4974	ADNI2	69.87	677.4	0.103	aCSF
*S_4976	ADNI2	62.4	905.6	0.069	aCSF
*S_4980	ADNI2	16.06	449.8	0.036	aCSF

*S_4982	ADNI2	40.66	692	0.059	aCSF
*S_4984	ADNI2	38.54	750.3	0.051	aCSF
*S_4986	ADNI2	11.27	780.5	0.014	nCSF
*S_4987	ADNI2	19.83	1091	0.018	nCSF
*S_4989	ADNI2	9.02	1087	0.008	nCSF
*S_4990	ADNI2	42	593.9	0.071	aCSF
*S_4992	ADNI2	18.42	418	0.044	aCSF
*S_5005	ADNI2	25.69	318.1	0.081	aCSF
*S_5006	ADNI2	66.53	653.9	0.102	aCSF
*S_5007	ADNI2	14.7	622	0.024	nCSF
*S_5012	ADNI2	33.95	458.3	0.074	aCSF
*S_5013	ADNI2	22.72	454.5	0.050	aCSF
*S_5014	ADNI2	13.24	585.6	0.023	nCSF
*S_5015	ADNI2	28.64	783.5	0.037	aCSF
*S_5017	ADNI2	54.78	622.5	0.088	aCSF
*S_5018	ADNI2	76.16	489.4	0.156	aCSF
*S_5019	ADNI2	36.63	587.9	0.062	aCSF
*S_5023	ADNI2	23.3	2081	0.011	nCSF
*S_5027	ADNI2	32.67	493.4	0.066	aCSF
*S_5028	ADNI2	49.99	437.6	0.114	aCSF
*S_5029	ADNI2	68.07	277.5	0.245	aCSF
*S_5037	ADNI2	25.91	700.9	0.037	aCSF
*S_5040	ADNI2	17.12	1879	0.009	nCSF
*S_5047	ADNI2	36.08	1001	0.036	aCSF
*S_5054	ADNI2	38.22	785.8	0.049	aCSF
*S_5058	ADNI2	14.76	255.5	0.058	aCSF
*S_5059	ADNI2	30.02	453.7	0.066	aCSF
*S_5062	ADNI2	74.14	542.4	0.137	aCSF
*S_5063	ADNI2	40.94	551.8	0.074	aCSF
*S_5070	ADNI2	19.45	489.7	0.040	aCSF
*S_5078	ADNI2	11.44	1321	0.009	nCSF
*S_5079	ADNI2	21.78	2667	0.008	nCSF
*S_5082	ADNI2	13.68	1600	0.009	nCSF
*S_5083	ADNI2	15.92	1002	0.016	nCSF
*S_5087	ADNI2	41.32	639.1	0.065	aCSF
*S_5091	ADNI2	24.08	1551	0.016	nCSF
*S_5093	ADNI2	21.86	2060	0.011	nCSF
*S_5095	ADNI2	34.29	382.5	0.090	aCSF
*S_5096	ADNI2	23.73	613.7	0.039	aCSF
*S_5100	ADNI2	12.93	1536	0.008	nCSF
*S_5102	ADNI2	24.23	1406	0.017	nCSF

*S_5109	ADNI2	17.63	771.9	0.023	nCSF
*S_5110	ADNI2	14	2008	0.007	nCSF
*S_5113	ADNI2	17.65	1762	0.010	nCSF
*S_5118	ADNI2	12.16	1210	0.010	nCSF
*S_5119	ADNI2	74.52	910.3	0.082	aCSF
*S_5124	ADNI2	30.81	2705	0.011	nCSF
*S_5125	ADNI2	14.06	1518	0.009	nCSF
*S_5127	ADNI2	21.87	469.2	0.047	aCSF
*S_5130	ADNI2	13.47	1687	0.008	nCSF
*S_5141	ADNI2	18.57	1923	0.010	nCSF
*S_5142	ADNI2	30.29	849.9	0.036	aCSF
*S_5147	ADNI2	26.23	2124	0.012	nCSF
*S_5153	ADNI2	20.68	2239	0.009	nCSF
*S_5157	ADNI2	15.83	1666	0.010	nCSF
*S_5169	ADNI2	26.06	1490	0.017	nCSF
*S_5178	ADNI2	20.96	1623	0.013	nCSF
*S_5185	ADNI2	45.64	662.8	0.069	aCSF
*S_5195	ADNI2	32.99	2571	0.013	nCSF
*S_5197	ADNI2	13.05	1142	0.011	nCSF
*S_5200	ADNI2	9.63	1112	0.009	nCSF
*S_5202	ADNI2	21.4	545.3	0.039	aCSF
*S_5213	ADNI2	25.87	3012	0.009	nCSF
*S_5219	ADNI2	28.83	1145	0.025	nCSF
*S_5228	ADNI2	21.07	1709	0.012	nCSF
*S_5230	ADNI2	22.84	1006	0.023	nCSF
*S_5242	ADNI2	27.06	1306	0.021	nCSF
*S_5243	ADNI2	14.2	1528	0.009	nCSF
*S_5252	ADNI2	27.87	474.9	0.059	aCSF
*S_5256	ADNI2	36.38	923.3	0.039	aCSF
*S_5258	ADNI2	26.32	869.7	0.030	aCSF
*S_5265	ADNI2	24.78	466.1	0.053	aCSF
*S_5266	ADNI2	24.28	2433	0.010	nCSF
*S_5272	ADNI2	25.05	2358	0.011	nCSF
*S_5277	ADNI2	34.39	780.3	0.044	aCSF
*S_5280	ADNI2	10.08	731.8	0.014	nCSF
*S_5287	ADNI2	26.11	2358	0.011	nCSF
*S_5289	ADNI2	15.79	1665	0.009	nCSF
*S_5292	ADNI2	36.39	928.3	0.039	aCSF
*S_5296	ADNI2	20.9	1460	0.014	nCSF
*S_0056	ADNIGO	15.18	1198	0.013	nCSF
*S_0059	ADNIGO	16.22	1616	0.010	nCSF

*S_0227	ADNIGO	28.45	323	0.088	aCSF
*S_0272	ADNIGO	23.79	1431	0.017	nCSF
*S_1030	ADNIGO	40.35	985.8	0.041	aCSF
*S_1117	ADNIGO	52.7	329.2	0.160	aCSF
*S_1261	ADNIGO	21.23	1711	0.012	nCSF
*S_2022	ADNIGO	22.11	929.2	0.024	nCSF
*S_2026	ADNIGO	9.42	1079	0.009	nCSF
*S_2042	ADNIGO	10.58	827.6	0.013	nCSF
*S_2045	ADNIGO	20.5	725.1	0.028	aCSF
*S_2047	ADNIGO	40.95	709.2	0.058	aCSF
*S_2055	ADNIGO	45.44	637.1	0.071	aCSF
*S_2063	ADNIGO	29.1	564.4	0.052	aCSF
*S_2068	ADNIGO	32.76	722.8	0.045	aCSF
*S_2073	ADNIGO	24.09	1094	0.022	nCSF
*S_2077	ADNIGO	18.71	859.1	0.022	nCSF
*S_2079	ADNIGO	48.48	518.6	0.093	aCSF
*S_2083	ADNIGO	13.69	1033	0.013	nCSF
*S_2087	ADNIGO	37.46	436.7	0.086	aCSF
*S_2100	ADNIGO	40.16	673.7	0.060	aCSF
*S_2106	ADNIGO	48.31	361.3	0.134	aCSF
*S_2109	ADNIGO	28.79	532.1	0.054	aCSF
*S_2121	ADNIGO	20.87	1016	0.021	nCSF
*S_2125	ADNIGO	15.85	638.6	0.025	nCSF
*S_2130	ADNIGO	30.39	476.6	0.064	aCSF
*S_2133	ADNIGO	28.71	413.9	0.069	aCSF
*S_2142	ADNIGO	32.49	632.1	0.051	aCSF
*S_2150	ADNIGO	24.9	731.4	0.034	aCSF
*S_2153	ADNIGO	10.4	980.4	0.011	nCSF
*S_2155	ADNIGO	82.04	539.6	0.152	aCSF
*S_2164	ADNIGO	12.57	1097	0.011	nCSF
*S_2167	ADNIGO	33.28	832	0.040	aCSF
*S_2171	ADNIGO	42.04	738.2	0.057	aCSF
*S_2190	ADNIGO	35.48	963.2	0.037	aCSF
*S_2194	ADNIGO	42.38	884.2	0.048	aCSF
*S_2195	ADNIGO	49.19	796	0.062	aCSF
*S_2196	ADNIGO	22.11	695.3	0.032	aCSF
*S_2201	ADNIGO	18.14	2282	0.008	nCSF
*S_2205	ADNIGO	23.28	336.6	0.069	aCSF
*S_2210	ADNIGO	11.79	316.1	0.037	aCSF
*S_2216	ADNIGO	23.14	530	0.044	aCSF
*S_2247	ADNIGO	14.24	858.9	0.017	nCSF

*S_2248	ADNIGO	66.72	646.9	0.103	aCSF
*S_2263	ADNIGO	13.19	776.9	0.017	nCSF
*S_2264	ADNIGO	21.16	839.5	0.025	nCSF
*S_2274	ADNIGO	25.43	476.5	0.053	aCSF
*S_2284	ADNIGO	15.13	791.6	0.019	nCSF
*S_2307	ADNIGO	32.58	741.3	0.044	aCSF
*S_2308	ADNIGO	11.78	982.6	0.012	nCSF
*S_2316	ADNIGO	69.57	589.6	0.118	aCSF
*S_2324	ADNIGO	9.8	832.9	0.012	nCSF
*S_2333	ADNIGO	23.45	662.6	0.035	aCSF
*S_2336	ADNIGO	33.64	909.4	0.037	aCSF
*S_2347	ADNIGO	24.18	1010	0.024	nCSF
*S_2367	ADNIGO	18.85	1086	0.017	nCSF
*S_2373	ADNIGO	68.61	779.8	0.088	aCSF
*S_2379	ADNIGO	10.58	804.8	0.013	nCSF
*S_2380	ADNIGO	21.81	696.5	0.031	aCSF
*S_2381	ADNIGO	57.7	684.7	0.084	aCSF
*S_2389	ADNIGO	11.73	881	0.013	nCSF
*S_2390	ADNIGO	38.61	892.1	0.043	aCSF
*S_2391	ADNIGO	19.78	412.7	0.048	aCSF
*S_2394	ADNIGO	17.5	360.4	0.049	aCSF
*S_2403	ADNIGO	24.66	572.4	0.043	aCSF

RID = ADNI Research Identification Number; pTau = cerebrospinal fluid (CSF) hyper phosphorylated tau; $A\beta_{1\text{-}42}$ = CSF measure of amyloid Beta (1-42 peptides), pTau/$A\beta_{1\text{-}42}$ = ratio of the hyperphsphorylated tau and amyloid Beta; Group CSF = CSF grouping strategy based on the pTau/ $A\beta_{1\text{-}42}$ ratio: aCSF = pTau/ $A\beta_{1\text{-}42}$ >= 0.028; nCSF = pTau/ $A\beta_{1\text{-}42}$ < 0.028. Aβ1-42 and pTau concentrations are in picograms per milliliter (pg/mL).

References

Aghourian M, Legault-Denis C, Soucy JP, Rosa-Neto P, Gauthier S, Kostikov A, et al. Quantification of brain cholinergic denervation in Alzheimer's disease using PET imaging with [18F]-FEOBV. Mol Psychiatry 2017

Aisen PS, Petersen RC, Donohue M, Weiner MW. Alzheimer's Disease Neuroimaging Initiative 2 Clinical Core: Progress and plans. Alzheimer's Dement 2015; 11: 734–739.

Aisen PS, Petersen RC, Donohue MC, Gamst A, Raman R, Thomas RG, et al. Clinical core of the Alzheimer's disease neuroimaging initiative: Progress and plans. Alzheimer's Dement 2010; 6: 239–246.

Amunts K, Kedo O, Kindler M, Pieperhoff P, Mohlberg H, Shah NJ, et al. Cytoarchitectonic mapping of the human amygdala, hippocampal region and entorhinal cortex: Intersubject variability and probability maps. Anat Embryol (Berl) 2005; 210: 343–352.

Ashburner J. A fast diffeomorphic image registration algorithm. Neuroimage 2007; 38: 95–113.

Ashburner J, Friston KJ. Unified segmentation. Neuroimage 2005; 26: 839–851.

Ashburner J, Ridgway GR. Symmetric diffeomorphic modeling of longitudinal structural MRI. Front Neurosci 2013; 6: 1–19.

Baker-Nigh A, Vahedi S, Davis EG, Weintraub S, Bigio EH, Klein WL, et al. Neuronal amyloid-β accumulation within cholinergic basal forebrain in ageing and Alzheimer's disease. Brain 2015; 138: 1722–1737.

Ballinger EC, Ananth M, Talmage DA, Role LW. Review Basal Forebrain Cholinergic Circuits and Signaling in Cognition and Cognitive Decline. Neuron 2016; 91: 1199–1218.

Bellucci A, Luccarini I, Scali C, Prosperi C, Giovannini MG, Pepeu G, et al. Cholinergic dysfunction, neuronal damage and axonal loss in TgCRND8 mice. Neurobiol Dis 2006

Braak H, Alafuzoff I, Arzberger T, Kretzschmar H, Tredici K. Staging of Alzheimer disease-associated neurofibrillary pathology using paraffin sections and immunocytochemistry. Acta Neuropathol 2006; 112: 389–404.

Braak H, Braak E. Neuropathological stageing of Alzheimer-related changes. Acta Neuropathol 1991; 82: 239–59.

Braak H, Del Tredici K. The pathological process underlying Alzheimer's disease in individuals under thirty. Acta Neuropathol 2011; 121: 171–181.

De Calignon A, Polydoro M, Suárez-Calvet M, William C, Adamowicz DH, Kopeikina KJ, et al. Propagation of Tau Pathology in a Model of Early Alzheimer's Disease. Neuron 2012
Cantero JL, Zaborszky L, Atienza M. Volume loss of the nucleus basalis of meynert is associated with atrophy of innervated regions in mild cognitive impairment. Cereb Cortex 2017; 27: 3881–3889.
Cavedo E, Grothe MJ, Colliot O, Lista S, Chupin M, Dormont Di, et al. Reduced basal forebrain atrophy progression in a randomized Donepezil trial in prodromal Alzheimer's disease. Sci Rep 2017; 7: 1–10.
Corder EH, Saunders AM, Strittmatter WJ, Schmechel DE, Gaskell PC, Small GW, et al. Gene dose of apolipoprotein E type 4 allele and the risk of Alzheimer's disease in late onset families. Science (80-) 1993; 261: 921–923.
Corder EH, Woodbury MA, Volkmann I, Madsen DK, Bogdanovic N, Winblad B. Density profiles of Alzheimer disease regional brain pathology for the Huddinge brain bank: Pattern recognition emulates and expands upon Braak staging. In: Experimental Gerontology. 2000. p. 851–864
Crane PK, Carle A, Gibbons LE, Insel P, Mackin RS, Gross A, et al. Development and assessment of a composite score for memory in the Alzheimer's Disease Neuroimaging Initiative (ADNI). Brain Imaging Behav 2012; 6: 502–516.
Diedenhofen B, Musch J. Cocor: A comprehensive solution for the statistical comparison of correlations. PLoS One 2015; 10: 1–12.
Gibbons. A composite score for executive functioning, validated in Alzheimer's Disease Neuroimaging Initiative (ADNI) participants with baseline mild cognitive impairment. Brain Imaging Behav 2012; 6: 517–527.
Grothe M, Heinsen H, Teipel S. Longitudinal measures of cholinergic forebrain atrophy in the transition from healthy aging to Alzheimer's disease. Neurobiol Aging 2013; 34: 1210–1220.
Grothe M, Heinsen H, Teipel SJ. Atrophy of the cholinergic basal forebrain over the adult age range and in early stages of Alzheimer's disease. Biol Psychiatry 2012; 71: 805–813.
Hall AM, Moore RY, Lopez OL, Kuller L, Becker JT. Basal forebrain atrophy is a presymptomatic marker for Alzheimer's disease. Alzheimer's Dement 2008; 4: 271–279.
Hansson O, Seibyl J, Stomrud E, Zetterberg H, Trojanowski JQ, Bittner T, et al. CSF biomarkers

of Alzheimer ' s disease concord with amyloid- b PET and predict clinical progression : A study of fully automated immunoassays in BioFINDER and ADNI cohorts. 2018: 1–12.
Harris JA, Devidze N, Verret L, Ho K, Halabisky B, Thwin MT, et al. Transsynaptic Progression of Amyloid-β-Induced Neuronal Dysfunction within the Entorhinal-Hippocampal Network. Neuron 2010; 68: 428–441.
Hayes AF. PROCESS: A versatile computational tool for observed variable mediation, moderation, and conditional process modeling. White Pap 2012: 1–39.
Iturria-Medina Y, Sotero RC, Toussaint PJ, Mateos-Pérez JM, Evans AC, Weiner MW, et al. Early role of vascular dysregulation on late-onset Alzheimer's disease based on multifactorial data-driven analysis. Nat Commun 2016; 7
Kfoury N, Holmes BB, Jiang H, Holtzman DM, Diamond MI. Trans-cellular propagation of Tau aggregation by fibrillar species. J Biol Chem 2012; 287: 19440–19451.
Khan UA, Liu L, Provenzano FA, Berman DE, Profaci CP, Sloan R, et al. Molecular drivers and cortical spread of lateral entorhinal cortex dysfunction in preclinical Alzheimer's disease. Nat Neurosci 2014; 17: 304–311.
De Lacalle S, Cooper JD, Svendsen CN, Dunnett SB, Sofroniew M V. Reduced retrograde labelling with fluorescent tracer accompanies neuronal atrophy of basal forebrain cholinergic neurons in aged rats. Neuroscience 1996
Liu C, Bu G. Apolipoprotein E and Alzheimer disease : risk , mechanisms and therapy. Nat Rev Neurol 2013
Liu L, Drouet V, Wu JW, Witter MP, Small SA, Clelland C, et al. Trans-synaptic spread of tau pathology in vivo. PLoS One 2012; 7
Ma D, Popuri K, Bhalla M, Jacova C, Wang L, Beg MF, et al. Quantitative Assessment of Field Strength , Total Intracranial Volume , Sex and Age on The Goodness of Harmonization For Volumetric Analysis on The ADNI Database Conclusion. 2018: 3–4.
Malone IB, Leung KK, Clegg S, Barnes J, Whitwell JL, Ashburner J, et al. Accurate automatic estimation of total intracranial volume: A nuisance variable with less nuisance. Neuroimage 2015; 104: 366–372.
Marchewka A, Kherif F, Krueger G, Grabowska A, Frackowiak R, Draganski B. Influence of magnetic field strength and image registration strategy on voxel-based morphometry in a study

of Alzheimer's disease. Hum Brain Mapp 2014
Mattson MP, Magnus T. Ageing and neuronal vulnerability. Nat Rev Neurosci 2006; 7: 278–294.
Mechelli A, Price CJ, Friston KJ, Ashburner J. Voxel-Based Morphometry of the Human Brain: Methods and Applications. 2005: 1–9.
Mesulam M -M, Geula C. Nucleus basalis (Ch4) and cortical cholinergic innervation in the human brain: Observations based on the distribution of acetylcholinesterase and choline acetyltransferase. J Comp Neurol 1988; 275: 216–240.
Mesulam M, Shaw P, Mash D, Weintraub S. Cholinergic nucleus basalis tauopathy emerges early in the aging-MCI-AD continuum. Ann Neurol 2004; 55: 815–828.
Mesulam MM. Cholinergic Innervation of Cortex by the Basal Forebrain: Cytochemistry and Cortical Connections of the Septa1 Area, Diagonal Band Nuclei, Nucleus Basalis (Substantia Innominata), and Hypothalamus in the Rhesus Monkey. 1983; 197
Morfini G, Pigino G, Atagi Y, Busciglio J, LaDu M, Yu C, et al. Disruption of fast axonal transport is a pathogenic mechanism for intraneuronal amyloid beta. Proc Natl Acad Sci 2009; 106: 5907–5912.
Nichols E. T, Holmes P. A. Nonparametric permutation tests for functional neuroimaging: A primer with examples. Hum Brain Mapp 2002; 15: 1–25.
Nitsch RM, Blusztajn JANK, Pittast AG, Slackt BE, Growdon JH, Wurtmant RJ. Evidence for a membrane defect in Alzheimer disease brain. 1992; 89: 1671–1675.
Petersen RC, Aisen PS, Beckett LA, Donohue MC, Gamst AC, Harvey DJ, et al. Alzheimer's Disease Neuroimaging Initiative (ADNI): Clinical characterization. Neurology 2010; 74: 201–209.
Poirier J. Apolipoprotein E in animal models of CNS injury and in alzheimer's disease. Trends Neurosci 1994; 17: 525–530.
Poirier J, Bertrand P, Poirier J, Kogan S, Gauthier S, Poirier J, et al. Apolipoprotein E polymorphism and Alzheimer's disease. Lancet 1993; 342: 697–699.
Poirier J, Delisle M-C, Quirion R, Aubert I, Farlow M, Lahiri D, et al. Apolipoprotein E4 allele as a predictor of cholinergic deficits and treatment outcome in Alzheimer disease. Proc Natl Acad Sci U S A 1995; 92: 12260–12264.

Roussarie J, Yao V, Plautz Z, Kasturia S, Albornoz C, Eric F, et al. Selective neuronal vulnerability in Alzheimer ' s disease: a network-based analysis. bioRxiv 2018: 1–14.
Saxena S, Caroni P. Selective Neuronal Vulnerability in Neurodegenerative Diseases: From Stressor Thresholds to Degeneration. Neuron 2011; 71: 35–48.
Saykin AJ, Shen L, Foroud TM, Potkin SG, Swaminathan S, Kim S, et al. Alzheimer's Disease Neuroimaging Initiative biomarkers as quantitative phenotypes: Genetics core aims, progress, and plans. Alzheimer's Dement 2010; 6: 265–273.
Schindler SE, Gray JD, Gordon BA, Xiong C, Batrla-utermann R, Quan M, et al. Cerebrospinal fluid biomarkers measured by Elecsys assays compared to amyloid imaging. Alzheimer's Dement 2018: 1–10.
Schmitz TW, Mur M, Aghourian M, Bedard MA, Spreng RN. Longitudinal Alzheimer's Degeneration Reflects the Spatial Topography of Cholinergic Basal Forebrain Projections. Cell Rep 2018; 24: 38–46.
Schmitz TW, Spreng RN. Basal forebrain degeneration precedes and predicts the cortical spread of Alzheimer's pathology. Nat Commun 2016; 7
Sepulcre J, Grothe MJ, d'Oleire Uquillas F, Ortiz-Terán L, Diez I, Yang HS, et al. Neurogenetic contributions to amyloid beta and tau spreading in the human cortex. Nat Med 2018
Shaw LM, Vanderstichele H, Knapik-Czajka M, Clark CM, Aisen PS, Petersen RC, et al. Cerebrospinal fluid biomarker signature in alzheimer's disease neuroimaging initiative subjects. Ann Neurol 2009; 65: 403–413.
Tamamaki N, Nojyo Y. Projection of the entorhinal layer II neurons in the rat as revealed by intracellular pressure-injection of neurobiotin. Hippocampus 1993; 3: 471–480.
Tan CH, Bonham LW, Fan CC, Mormino EC, Sugrue LP, Broce IJ, et al. Polygenic hazard score, amyloid deposition and Alzheimer's neurodegeneration. Brain 2019: 1–11.
Tardif CL, Collins DL, Pike GB. Regional impact of field strength on voxel-based morphometry results. Hum Brain Mapp 2010; 31: 943–957.
Veitch DP, Weiner MW, Aisen PS, Beckett LA, Cairns NJ, Green RC, et al. Understanding disease progression and improving Alzheimer's disease clinical trials: Recent highlights from the Alzheimer's Disease Neuroimaging Initiative. Alzheimer's Dement 2018: 1–46.
Walker LC, Diamond MI, Duff KE, Hyman BT. Mechanisms of protein seeding in

neurodegenerative diseases. JAMA Neurol 2013; 70: 304–310.
Warren JD, Rohrer JD, Schott JM, Fox NC, Hardy J, Rossor MN. Molecular nexopathies: A new paradigm of neurodegenerative disease. Trends Neurosci 2013; 36: 561–569.
Wu H, Williams J, Nathans J. Complete morphologies of basal forebrain cholinergic neurons in the mouse. Elife 2014; 2014: 1–17.
Wu JW, Hussaini SA, Bastille IM, Rodriguez GA, Mrejeru A, Rilett K, et al. Neuronal activity enhances tau propagation and tau pathology in vivo. Nat Neurosci 2016; 19: 1085–1092.
Wurtman RJ. Choline metabolism as a basis for the selective vulnerability of cholinergic neurons. Trends Neurosci 1992; 15: 117–122.
Wyman BT, Harvey DJ, Crawford K, Bernstein MA, Cole PE, Crane P, et al. Standardization of Analysis Sets for Reporting Results from ADNI MRI Data. 2014; 9: 332–337.
Zaborszky L, Hoemke L, Mohlberg H, Schleicher A, Amunts K, Zilles K. Stereotaxic probabilistic maps of the magnocellular cell groups in human basal forebrain. Neuroimage 2008; 42: 1127–1141.